EPRI
Electric Power
Research Institute

Keywords:
Effective dose equivalent
Radiation exposure
Photon radiation
Dosimetry
10 CFR 20

EPRI TR-101909-V2
Project RP3099-10
Final Report
June 1995

Assessment of the Effective Dose Equivalent for External Photon Radiation

Volume 2: Calculational Techniques for Estimating External Effective Dose Equivalent from Dosimeter Readings

Prepared by
Texas A&M University

REPORT SUMMARY

Assessment of the Effective Dose Equivalent for External Photon Radiation

Volume 2: Calculational Techniques for Estimating External Effective Dose Equivalent from Dosimeter Readings

Recent revisions to the radiation protection standards contained in Title 10 Part 20 of the Code of Federal Regulations require nuclear power plants to assess a worker's "effective dose equivalent" (EDE). This report explains the concept of effective dose equivalent and describes research to improve the dosimetric methods presently used for assessing EDE.

INTEREST CATEGORIES

Radiation protection technology
Radiation field control
Low level radioactive waste management

KEYWORDS

Effective dose equivalent
Radiation exposure
Photon radiation
Dosimetry
10 CFR 20

BACKGROUND In 1977, to account for human organ and tissue differences, the International Commission on Radiological Protection (ICRP), proposed specific organ radiation exposure weighting factors—in essence, risk-based radiation dose limits. These and other aspects of the ICRP recommendations were adopted in revisions made in 1991 to 10 CFR 20. The regulations require licensees to evaluate radiation exposures in terms of EDE using the conservative assumption that the weighting factor for external exposure is one. However, the regulations allow licensees to propose alternative methods for evaluating the external radiation component of effective dose equivalent. This report tabulates EDE under a broad variety of radiation exposure situations and examines dosimeter placement and how well isotropic dosimeters measure EDE. Utilities can use this data to evaluate various ways to meet effective dose equivalent regulations.

OBJECTIVES

- To describe EPRI's effective dose equivalent research
- To explain the enhanced methodology being developed by EPRI for assessing effective dose equivalent at nuclear power plants

APPROACH Researchers performed Monte Carlo calculations of photon transport through the human body. They used mathematical models of the human adult male and female and, for a variety of external radiation sources, calculated energy deposition in a large number of human organs and tissues. Using published organ weighting factors, they calculated effective dose equivalents for these irradiations. They determined how EDE varies with photon energy for various beam source geometries, and for point sources both on and off the body. Calculations were made of photon energy fluence on the surface of the body as a function of location, source geometry, and photon energy. This allowed researchers to understand how dosimeter placement effects EDE assessments.

RESULTS For beam sources, beams striking the front of the body normal to the body's major axis (i.e., straight on) produce the largest effective dose equivalent. The next highest effective dose equivalent are produced by beams striking the rear of the torso, again normal to the body's major axis. Effective dose equivalent falls significantly if the incident radiation departs from these two orientations. For point sources in contact with the body, the effective dose equivalent is highest for females when the source is on the front of the torso near the sternum. For males, it is

highest when the source is on the front of the torso near the gonads. The widespread practice of supplementing a single front-worn dosimeter with additional dosimeters placed facing a radiation source should be abandoned, as this can significantly overestimate EDE. Using a single front-worn dosimeter as a measure of EDE is acceptable. Simple algorithms applied to two dosimeters (on the front and back) yield a more accurate and numerically lower EDE under all radiation exposure situations.

EPRI PERSPECTIVE Considerable benefits can be derived by U.S. nuclear utilities if they develop a technically rigorous approach for determining effective dose equivalents for their workforces. Their approach should be generally conservative, be acceptable to regulatory agencies, and be consistent with existing dosimetry practices. This report (Volume 2 of a two-part study) presents a methodology for meeting these objectives. EPRI will continue to work closely with member utilities, industry groups, and regulators to review, verify, and validate this approach. EPRI's goal is an accurate effective dose equivalent methodology that can be implemented using existing technologies.

PROJECT
RP3099-10
EPRI Project Manager: Carol Hornibrook
Low-Level Waste, Chemistry and Radiation Control
Nuclear Power Group
Contractors: Texas A&M University; ENCORE Technical Resources, Inc.

Assessment of the Effective Dose Equivalent for External Photon Radiation

Volume 2: Calculational Techniques for Estimating External Effective Dose Equivalent from Dosimeter Readings

TR-101909-V2
Research Project 3099-10

Final Report, June 1995

Prepared by
Texas A&M University
College Station, TX 77843-3133

Principal Investigators
W. D. Reece
J. W. Poston
X. George Xu

Edited by
ENCORE Technical Resources, Inc.
141 North Spring Street
Middletown, PA 17057

D. E. Owen

Prepared for
Electric Power Research Institute
3412 Hillview Avenue
Palo Alto, California 94304

EPRI Project Manager
C. Hornibrook

Low-Level Waste, Chemistry and Radiation Control
Nuclear Power Group

DISCLAIMER OF WARRANTIES AND LIMITATION OF LIABILITIES

ORGANIZATION THAT PREPARED THIS REPORT:

TEXAS A&M UNIVERSITY

ORDERING INFORMATION

Requests for copies of this report should be directed to EPRI Distribution Center, 207 Coggins Drive, P.O. Box 23205, Pleasant Hill, CA 94523, (510) 934-4212.

ABSTRACT

U.S. nuclear power plants have recently changed the way they determine radiation exposure to their workforce. Revisions to Title 10 Part 20 of the Code of Federal Regulations now require licensees to evaluate worker radiation exposure using a risk-based methodology termed *effective dose equivalent*. Effective dose equivalent is intended to be a measure of an individual's potential risk of stochastic injury from ionizing radiation exposure, in particular, the potential risk of fatal cancer to the individual or genetic defects in his or her progeny. Effective dose equivalent is based on known variations in sensitivity to radiation of the various organs of the body. By accounting for these variations, effective dose equivalent yields a measure of radiation exposure that is proportional to risk.

A research project was undertaken to improve the methods presently used for assessing effective dose equivalent. In this project effective dose equivalent was calculated using a mathematical model of the human body and tracking photon interactions for a wide variety of radiation source geometries using Monte Carlo computer code simulations. Algorithms were then developed to relate measurements of photon energy fluence on the surface of the body (as measured by dosimeters) to effective dose equivalent. An earlier report (Volume 1 of this study) described:

- the concept of effective dose equivalent
- the evolution of the concept and its incorporation into regulations
- the variations in human organ susceptibility to radiation
- the mathematical modeling and calculational techniques used to assess effective dose equivalent
- the results of effective dose equivalent calculations for males and females for a broad range of photon energies and source geometries.

This report (the second and final volume of the study) presents:

- calculations of photon energy fluence on the surface of the human body for a range of photon energies and source geometries
- algorithms derived from the energy fluence calculations and Volume 1 results that can be applied to standard dosimeter readings to more accurately calculate effective dose equivalent

- a comparison of effective dose equivalent measurements made using a physical model of the human torso with effective dose equivalent calculated by algorithm (under both laboratory and field conditions at a nuclear power plant)
- a discussion of the angular dependence of dosimeter readings and recommendations on how to correct for angular dependence to reduce errors in calculating effective dose equivalent.

ACKNOWLEDGMENTS

The following individuals served as technical advisors to EPRI for this project, and as such reviewed the manuscript and made many helpful recommendations:

- Ralph Anderson (Nuclear Energy Institute)
- Patrick Hughes (Arizona Public Service Company)
- John J. Kelly (New York Power Authority)
- Nora Nicholson (Nuclear Energy Institute)
- John Schmitt (Nuclear Energy Institute)
- Michael C. Williams (Union Electric Company).

Battelle Pacific Northwest Laboratories conducted the RANDO phantom irradiation experiments. EPRI thanks Rochester Gas and Electric Corporation for allowing the instrumented phantom to be exposed to power plant radiation fields at their R.E. Ginna nuclear power station.

CONTENTS

Section Page

LIST OF FIGURES

LIST OF TABLES

1.0 INTRODUCTION

1.1 The Purpose of This Study

The work reported herein culminates several years of research sponsored by the Electric Power Research Institute (EPRI). EPRI undertook this research on behalf of member utilities in response to fundamental changes made in federal radiation protection regulations. Title 10 Part 20 of the Code of Federal Regulations ("Standards for Protection Against Radiation") was revised in 1991.[1] Among other changes, the revised regulations add the concept of *effective dose equivalent,* and require that certain effective dose equivalent limits not be exceeded. This requirement is the subject of this report.

Readers unfamiliar with effective dose equivalent and its origins may want to review Volume 1 of this study[2] which defined effective dose equivalent, described how it is calculated, and discussed the history and evolution of the concept. Very briefly, effective dose equivalent is a radiation protection philosophy based on:

- the observation that radiation can cause stochastic (random) effects in the human body, such as cancer in exposed individuals or genetic defects in the progeny or subsequent generations of those exposed
- the observation that human organs and tissues differ in their susceptibility to stochastic effects
- the idea that this difference in susceptibility can be accounted for by assigning radiation effects weighting factors to the various organs and tissues, and then summing the results over all organs and tissues to obtain a measure of the combined effect.

The effective dose equivalent is the sum of the effective dose equivalents for individual organs and tissues (designated by the subscript i) multiplied by their respective weighting factors.

$$H_E = \sum H_{Ei} = \sum w_{Ti} \times H_{Ti} \qquad \text{Eq. 1}$$

A simple example illustrates the concept. Imagine a situation (say a medical treatment) where all the radiation is received by a single organ or tissue. In the

case of one individual it was low energy photons irradiating bone surfaces, in the case of another the lungs were irradiated. The prescribed weighting factors are 0.03 for bone surfaces and 0.12 for the lungs. This means the bone patient can receive four times the radiation dose of the lung patient, and both will have the same potential risk of death from cancer from their treatments.*

This approach had its origins in a 1977 publication by the International Commission on Radiological Protection (ICRP).[3] That publication—ICRP-26—introduced a variety of new radiation protection concepts, including the concept of risk-based dose limits for stochastic effects. For stochastic effects the ICRP recommended exposure limits based on the sum of the risks to individual organs (or tissues) of the body. They also specified the weighting factors to be applied to individual organ doses to account for differences in cellular radio-sensitivity, variations in susceptibility to stochastic effects, and variations in the treatability and lethality of different cancers. This approach supports the principle that risk should be equal, whether the body is irradiated uniformly or receives localized irradiation. In addition, this approach has the advantage that as radiation effects knowledge improves, weighting factors can be periodically updated.

The revised regulations that took effect in January 1994 specify that a worker's annual total effective dose equivalent not exceed 5 rem. (Other limits are also specified, including dose to individual organs, the lens of the eye, and the skin. But these limits are not applicable to this discussion.) The regulations require that total effective dose equivalent be calculated by summing the external component (called by various terms, including deep-dose equivalent** and dose equivalent) and the internal component (called the committed*** effective dose equivalent).

---

* Strictly speaking, the weighting factors from 10 CFR 20 do not apply to medical treatments. The medical treatment analogy is used here merely to illustrate the example of single organ exposures.

** The dose equivalent at a tissue depth of 1 cm (1,000 mg / cm^2)

*** The term "committed" is used because internal radiation "commits" the body to receiving future exposure, and this future exposure must be accounted for.

Practically, one cannot place dosimeters over the body's entire surface or inside individual organs in order to measure ionizing radiation. Rather, one must use calculational methods—algorithms—to evaluate effective dose equivalent from external and internal radiation sources. To assess the risk of radiation to organs and tissues one must know from where the radiation is emanating, the properties of that radiation (type, energy, etc.), the organs' differing sensitivities to radiation, and the shielding effects of the body itself. This knowledge—coupled with actual dosimeter measurements at specific locations on the body (for external exposures) or airborne concentrations or bioassay measurements (for internal exposures)—makes it possible to assess total effective dose equivalent.

The purpose of this research is to develop a calculation technique for more accurately assessing the external component to total effective dose equivalent from ionizing photon radiation (x- and gamma rays). Since the vast majority of exposures at nuclear power plants involve external exposures only, accurate (and not excessively conservative) assessments of these exposures are particularly important to workers and utilities. Accurate effective dose equivalent assessments will:

- provide a basis for optimizing worker protection practices, and
- provide better data for ongoing evaluation of the potential risks associated with radiation exposure.

1.2 Report Organization

Section 2 provides a brief summary of the results from Volume 1 of this study, which presented calculations of effective dose equivalent for males and females exposed to external radiation from both beam and point sources. Section 3 presents calculations of photon energy fluence on the surface of the body for the beam and point sources used in Volume 1. Section 4 relates these surface fluence measurements to the effective dose equivalents calculated in the earlier study, and derives algorithms for calculating effective dose equivalent from one or more surface fluence measurements. Measurements of effective dose equivalent made in the laboratory and at a commercial nuclear reactor are also presented, and are compared to effective dose equivalent values calculated using the derived algorithms. Section 5 summarizes the above information and recommends a

methodology for more accurately assessing effective dose equivalent for nuclear plant workers exposed to external ionizing radiation.

The sections that follow assume the reader is generally familiar with:

- weighting factors that account for variations in sensitivity of organs and tissues to ionizing radiation
- mathematical models to depict the internal structure of the human body
- Monte Carlo photon transport computer codes to calculate how radiation interacts with the human body.

Readers unfamiliar with these concepts may wish to review Section 2 of the first volume of this study.[2] Knowledge of the organ weighting factors is particularly important to subsequent discussions in this report. Accordingly, weighting factors are summarized in Table 1. Readers may also wish to review the discussion in reference 2 about gender-specific weighting factors and how they relate to the weighting factors specified in 10 CFR 20.

Table 1. Gender-Specific Organ Weighting Factors (w_T)

Organ	Male	Female	10 CFR 20
Gonads	0.25	0.25	0.25
Breast	0.00	0.30	0.15
Lung	0.12	0.10	0.12
Red Marrow	0.12	0.10	0.12
Thyroid	0.02	0.04	0.03
Bone Surface	0.03	0.03	0.03
Remainder	0.30	0.30	0.30
Totals	0.84	1.12	1.00

2.0 EFFECTIVE DOSE EQUIVALENT FROM BEAM AND POINT SOURCES

2.1 Overview

The results presented in this section are based on Monte Carlo computer code calculations of photon transport through anthropomorphic phantoms (mathematical models of the human body). In this approach, the human body is mathematically modeled and the behavior of a very large number of incident photons striking the body is calculated. The mathematical models used were developed by Cristy and Eckerman[4], representing a standard adult male and female. Each phantom consists of three major sections (Figure 1):

- the trunk and arms (represented by an elliptical cylinder)
- the legs and feet (represented by two truncated circular cones)
- the head and neck (represented by an elliptical cylinder capped by half an ellipsoid).

The various organs are modeled geometrically and assigned one of three tissues: skeletal, lung, or soft tissue. The models consist of a large number of equations, each describing a particular anatomical feature of the phantom. These equations are accompanied by tables that list numerical factors and coefficients used to construct a particular feature for either males or females.

The Monte Carlo radiation transport code selected for this study—MCNP (Monte Carlo Neutron-Photon)[5]—is extensively documented and has been used by researchers throughout the world to run tens-of-thousands of practical problems. Additional details on the phantoms and descriptions of how the MCNP code was run and the data were processed are in reference 2.

Since effective dose equivalent (H_E) is a slowly varying function of photon energy, calculations need only be done at a few energies to effectively map the results; other energies can be interpolated. For this study, three photon energies—0.08, 0.3, and 1.0 MeV—were used with each gender phantom to map the response for a given exposure geometry. (These energies adequately bound the photon energies encountered in a nuclear power facility.) For each phantom and each energy, a series of geometries were calculated. First, effective dose equivalents from beam sources for many three-dimensional angles of incidence

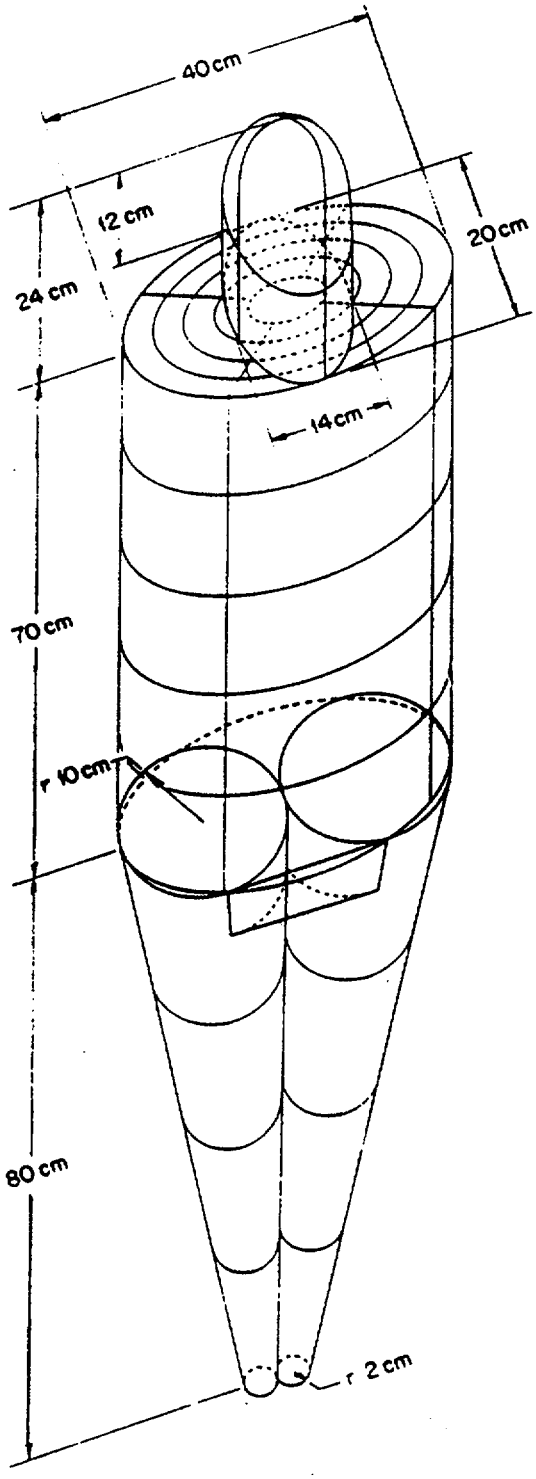

Figure 1. Exterior of the adult male phantom

were calculated. These were done at sufficient angular intervals so that effective dose equivalent and individual organ doses could be calculated by interpolation for any beam angle. Next, effective dose equivalents from point sources at various distances from the phantoms (ranging from contact to three meters) were calculated.

2.2 Beam Source Results

Beams, which irradiate uniformly across the height of the torso, are commonly encountered radiation sources that are easy to understand and characterize. All finite sources behave more like point sources as the distance between the source and the receptor increases. As this distance increases, the sources behave like beams, with the photons arriving ever more parallel. Thus, if we understand beam sources, we understand the limiting case for all other finite sources.

A standard polar-azimuthal angle system was used for naming the three-dimensional angles that describe the incident beam (see Figure 2). Polar angles run from 0° (beams directly overhead) to 180° (beams directly underfoot). Looking down on the torso from above, azimuthal angles run clockwise from 0° (beams incident on the front of the torso), to 180° (beams incident on the rear of the torso), and continuing around the torso to 360° (beams again incident on the front). Beams striking the torso from the front are termed *anterior-posterior* beams (abbreviated AP) . Beams striking the torso from the rear are termed *posterior-anterior* beams (abbreviated PA). And beams striking the torso from the side are termed *lateral* beams (abbreviated LAT). These irradiation geometries are illustrated in Figure 3.

The effect of beam direction on effective dose equivalent was mapped through all three-dimensional angles. Well over 100 beam angles were calculated, providing sufficient detail to allow simple interpolation through any two adjacent angles. Figures 4 and 5 summarize the results for radiation beams traversing the principal azimuthal and polar great circles. In order to make these figures easier to interpret, we have added small human icons to the top of each one. The location and orientation of these human icons on the figure is important. Their location corresponds to the azimuthal or polar angles shown on

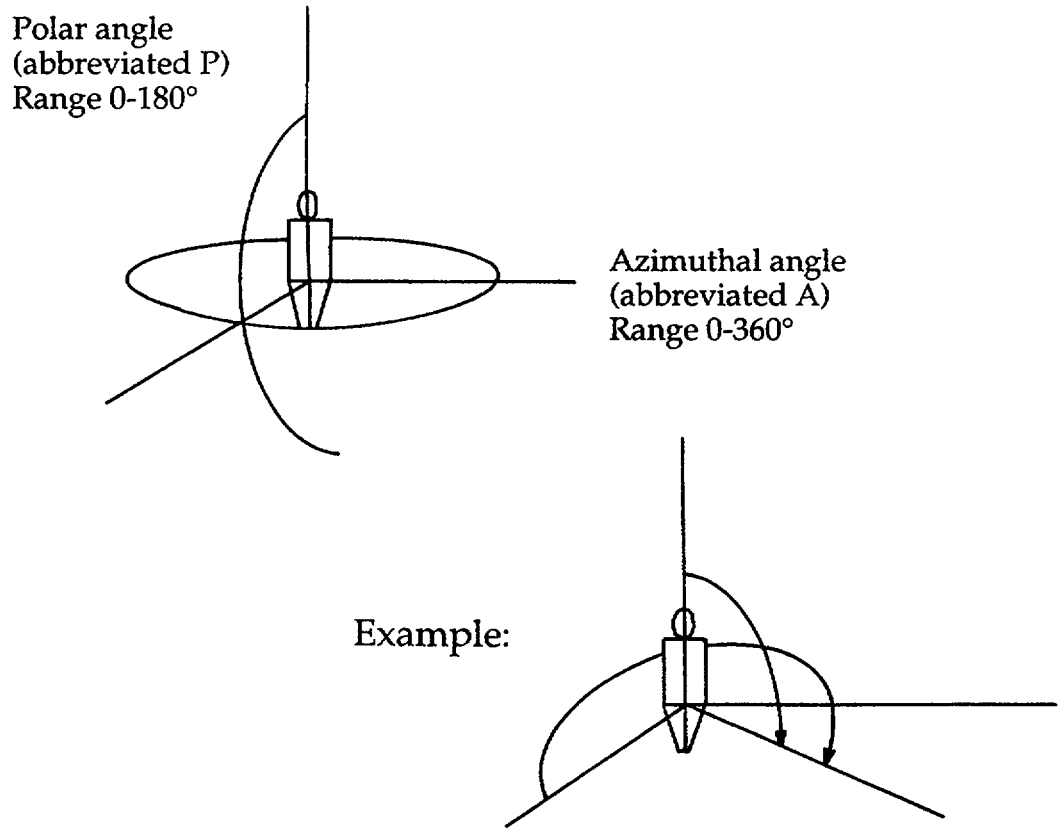

Figure 2. Nomenclature used to describe the beam angle of incidence

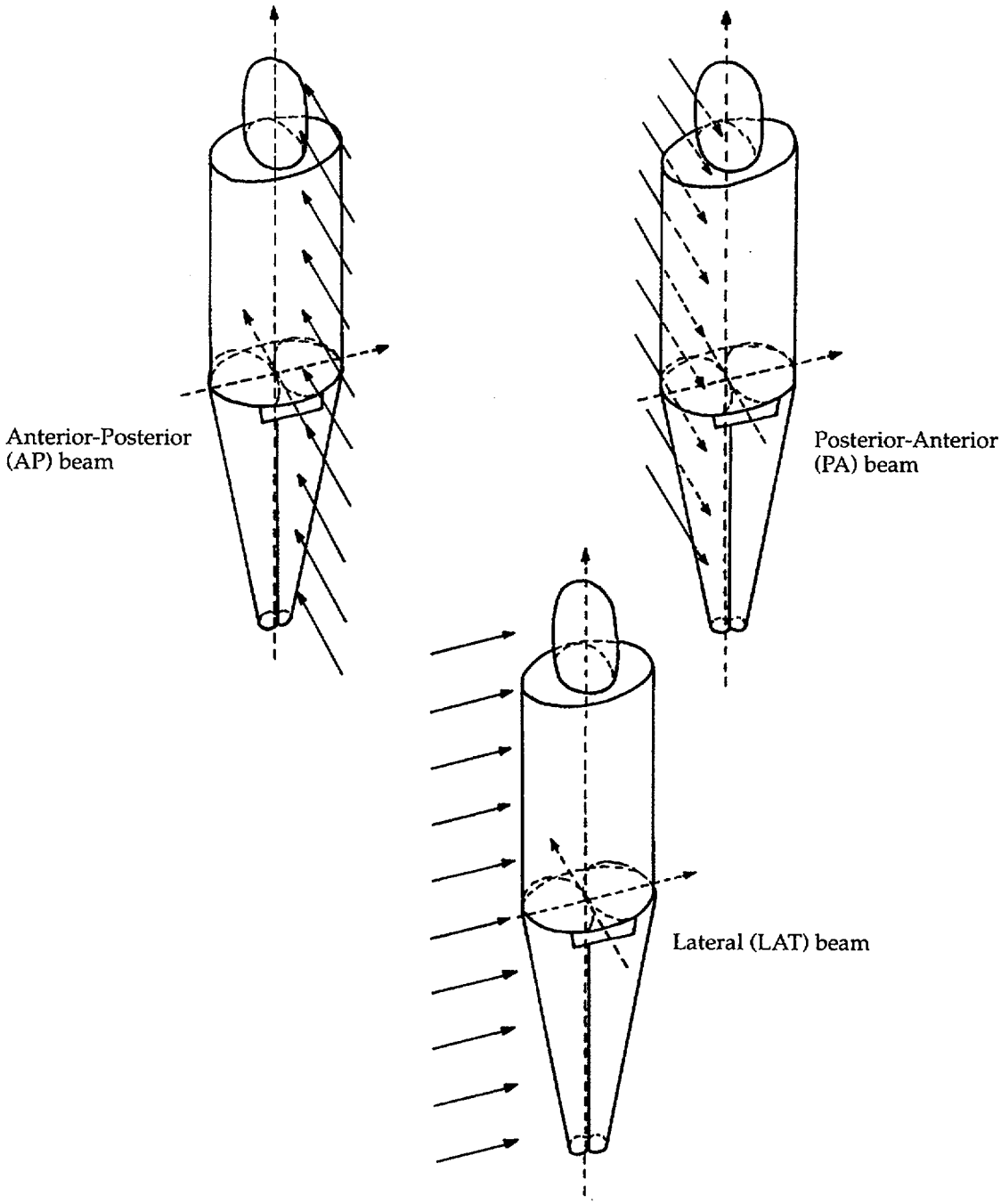

Figure 3. Phantom irradiation geometries

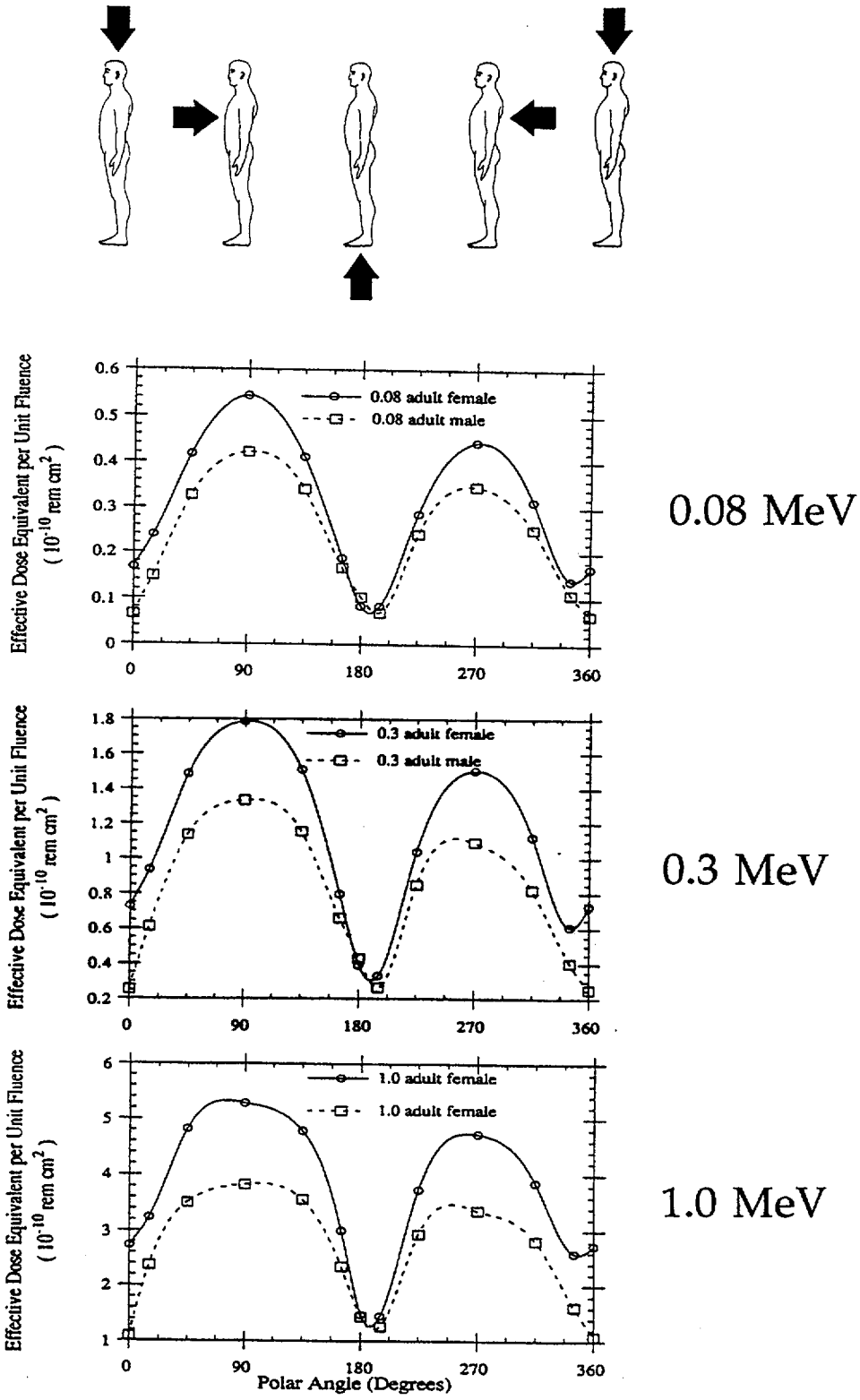

Figure 4. Effective dose equivalent vs. polar angle

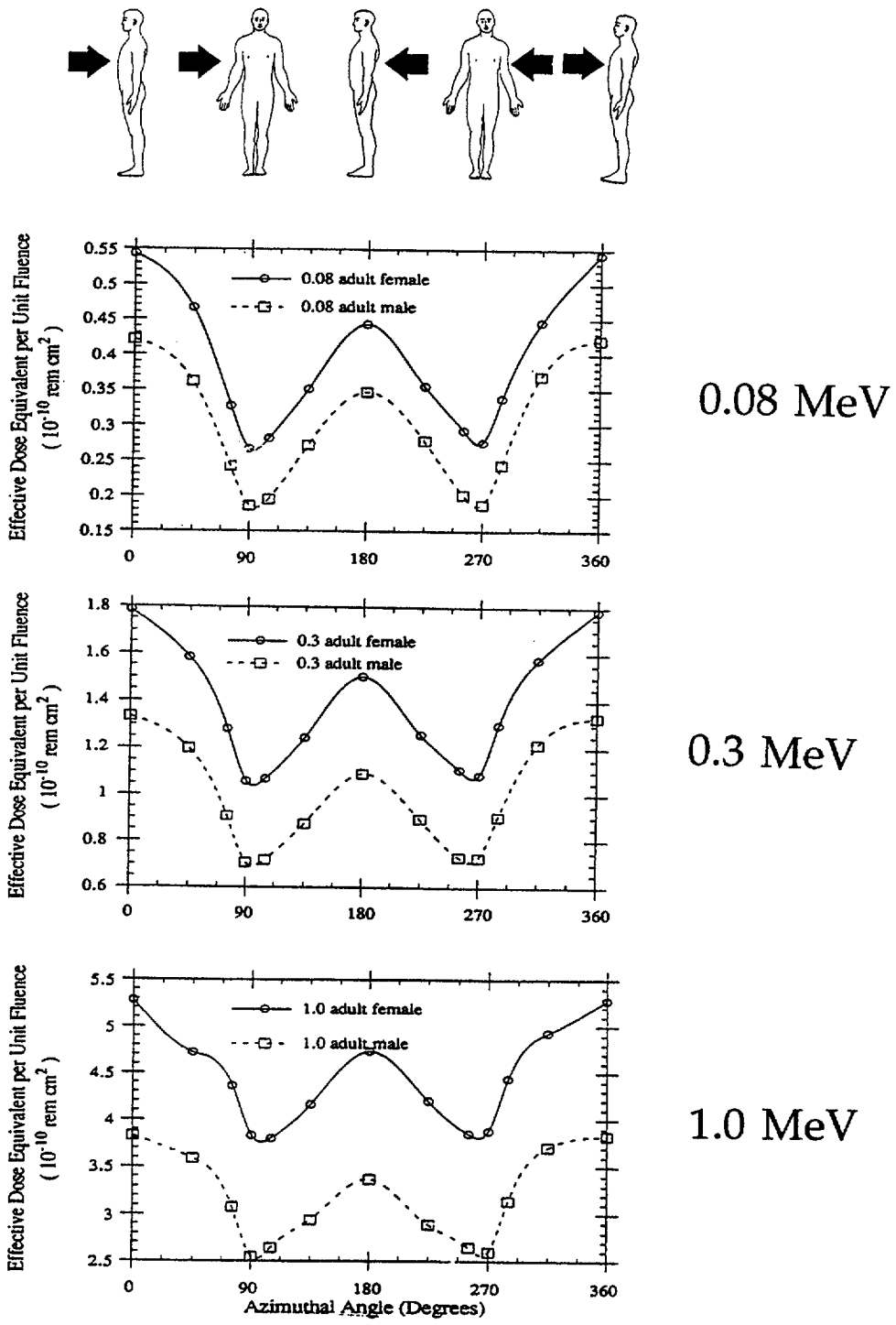

Figure 5. Effective dose equivalent vs. azimuthal angle

the figure, and their orientation gives the reader a quick reminder of the way the radiation beam is striking the phantom.

Figure 4 shows the variation of H_E as a function of photon energy, gender, and azimuthal angle, with the polar angle fixed at 90° (normal to the body's major axis). Figure 5 shows the variation of H_E as a function of photon energy, gender, and polar angle, with the azimuthal angle fixed at 0°-180° (normal to the body's major axis). These plots are only a small sampling of the data collected from the beam studies. Figures similar to these could be drawn for many other great circles covering the full spectrum of azimuthal and polar angles. Tables 2 through 4 present the data for all polar and azimuthal angles calculated.

Several important results are apparent from the beam data. Beams striking the torso normal to the body's major axis (AP or PA beams) produce the largest H_E. In all cases, H_E is higher for beams striking the front of the torso (AP) than for beams striking the rear of the torso (PA). Effective dose equivalent decreases dramatically as one departs from the AP or PA orientation. Although concern has been expressed in the literature about underfoot and overhead sources, the actual effective dose equivalent drops markedly for these geometries.*

For equivalent energy fluxes, lower energy photons always produce lower effective dose equivalents. This arises primarily from shielding of the deeper organs and the part of the torso away from the beam by parts of the body proximate to the beam. This is contrary to flux-to-dose relationships published in 1977 by ANSI[6] and used throughout the nuclear industry (see Figure 6). Because the ANSI Standard is based on maximum dose 1-cm deep in tissue, there appears to be a minimum in the flux-to-dose conversion at about 80 keV, with the conversion factor increasing both above and below this value. However, flux-to-dose conversions based on effective dose equivalent decrease monotonically with energy (see lower curve in Figure 6). Thus, the 1977 ANSI standard greatly over-predicts dose for low energy photons.

---

* Additional research on underfoot sources may be required because the results herein may be influenced by the mathematical phantom model. Note (Figure 1) that the legs of the model are represented by two truncated cones that touch. In this model radiation must pass through all of the leg structure before it reaches the gonads. A "legs apart' model would be a more accurate human representation.

Table 2. Effective Dose Equivalent for 0.08 MeV Photon Beams as a Function of Polar and Azimuthal Angle (units = E-10 rem-sq cm)

Adult Female

Polar Angle	0°	15°	45°	90°	135°	165°	180°
Azimuthal Angle							
0°	0.167	0.238	0.417	0.543	0.410	0.188	0.083
45°	0.167	0.221	0.349	0.466	0.336	0.165	0.083
75°	0.167	0.186	0.275	0.327	0.240	0.130	0.083
90°	0.167	0.168	0.232	0.266	0.190	0.103	0.083
105°	0.167	0.144	0.221	0.281	0.182	0.080	0.083
135°	0.167	0.135	0.258	0.351	0.220	0.071	0.083
180°	0.167	0.141	0.314	0.443	0.286	0.083	0.083
225°	0.167	0.135	0.263	0.355	0.241	0.073	0.083
255°	0.167	0.145	0.223	0.293	0.192	0.084	0.083
270°	0.167	0.168	0.241	0.276	0.198	0.106	0.083
285°	0.167	0.190	0.283	0.338	0.235	0.133	0.083
315°	0.167	0.217	0.355	0.446	0.335	0.166	0.083
360°	0.167	0.238	0.417	0.543	0.410	0.188	0.083

Adult Male

Polar Angle	0°	15°	45°	90°	135°	165°	180°
Azimuthal Angle							
0°	0.065	0.148	0.327	0.421	0.340	0.167	0.103
45°	0.065	0.118	0.270	0.362	0.276	0.146	0.103
75°	0.065	0.085	0.177	0.242	0.187	0.117	0.103
90°	0.065	0.076	0.139	0.186	0.116	0.082	0.103
105°	0.065	0.079	0.147	0.195	0.115	0.038	0.103
135°	0.065	0.092	0.204	0.272	0.182	0.049	0.103
180°	0.065	0.111	0.252	0.347	0.241	0.069	0.103
225°	0.065	0.095	0.208	0.278	0.189	0.051	0.103
255°	0.065	0.080	0.147	0.202	0.123	0.039	0.103
270°	0.065	0.077	0.145	0.188	0.119	0.088	0.103
285°	0.065	0.086	0.184	0.244	0.184	0.117	0.103
315°	0.065	0.119	0.271	0.370	0.273	0.149	0.103
360°	0.065	0.148	0.327	0.421	0.340	0.167	0.103

Table 3. Effective Dose Equivalent for 0.3 MeV Photon Beams as a Function of Polar and Azimuthal Angle (units = E-10 rem-sq-cm)

Adult Female

Polar Angle	0°	15°	45°	90°	135°	165°	180°
Azimuthal Angle							
0°	0.727	0.936	1.483	1.785	1.507	0.796	0.392
45°	0.727	0.872	1.341	1.584	1.276	0.704	0.392
75°	0.727	0.791	1.087	1.283	0.979	0.559	0.392
90°	0.727	0.706	0.931	1.059	0.796	0.448	0.392
105°	0.727	0.593	0.888	1.068	0.749	0.341	0.392
135°	0.727	0.542	0.949	1.245	0.863	0.284	0.392
180°	0.727	0.608	1.122	1.503	1.038	0.329	0.392
225°	0.727	0.536	0.976	1.259	0.900	0.291	0.392
255°	0.727	0.590	0.880	1.110	0.784	0.349	0.392
270°	0.727	0.706	0.950	1.086	0.830	0.454	0.392
285°	0.727	0.778	1.112	1.301	0.968	0.568	0.392
315°	0.727	0.875	1.318	1.575	1.290	0.693	0.392
360°	0.727	0.936	1.483	1.785	1.507	0.796	0.392

Adult Male

Polar Angle	0°	15°	45°	90°	135°	165°	180°
Azimuthal Angle							
0°	0.255	0.610	1.137	1.333	1.155	0.659	0.429
45°	0.255	0.505	1.005	1.199	0.999	0.576	0.429
75°	0.255	0.344	0.715	0.908	0.761	0.483	0.429
90°	0.255	0.297	0.547	0.707	0.499	0.353	0.429
105°	0.255	0.286	0.542	0.717	0.467	0.151	0.429
135°	0.255	0.337	0.691	0.872	0.623	0.183	0.429
180°	0.255	0.405	0.821	1.092	0.850	0.264	0.429
225°	0.255	0.336	0.708	0.895	0.654	0.198	0.429
255°	0.255	0.290	0.555	0.732	0.486	0.162	0.429
270°	0.255	0.291	0.579	0.728	0.503	0.365	0.429
285°	0.255	0.351	0.733	0.905	0.752	0.466	0.429
315°	0.255	0.488	1.003	1.219	0.977	0.583	0.429
360°	0.255	0.610	1.137	1.333	1.155	0.659	0.429

Table 4. Effective Dose Equivalent for 1.00 MeV Photon Beams as a Function of Polar and Azimuthal Angle (units = E-10 rem-sq cm)

Adult Female

Polar Angle	0°	15°	45°	90°	135°	165°	180°
Azimuthal Angle							
0°	2.730	3.240	4.820	5.280	4.780	3.000	1.480
45°	2.730	3.090	4.320	4.720	4.350	2.730	1.480
75°	2.730	2.870	3.870	4.360	3.580	2.110	1.480
90°	2.730	2.690	3.450	3.830	3.140	1.720	1.480
105°	2.730	2.310	3.340	3.800	2.860	1.380	1.480
135°	2.730	2.240	3.480	4.160	3.280	1.310	1.480
180°	2.730	2.590	3.860	4.730	3.740	1.450	1.480
225°	2.730	2.220	3.590	4.200	3.320	1.360	1.480
255°	2.730	2.330	3.280	3.850	3.010	1.400	1.480
270°	2.730	2.670	3.470	3.880	3.260	1.760	1.480
285°	2.730	2.890	3.940	4.440	3.550	2.130	1.480
315°	2.730	3.110	4.410	4.930	4.270	2.680	1.480
360°	2.730	3.240	4.820	5.280	4.780	3.000	1.480

Adult Male

Polar Angle	0°	15°	45°	90°	135°	165°	180°
Azimuthal Angle							
0°	1.090	2.370	3.510	3.830	3.560	2.350	1.440
45°	1.090	2.070	3.280	3.590	3.200	2.120	1.440
75°	1.090	1.520	2.680	3.080	2.710	1.680	1.440
90°	1.090	1.270	2.260	2.550	2.090	1.440	1.440
105°	1.090	1.190	2.140	2.640	2.000	0.810	1.440
135°	1.090	1.390	2.470	2.940	2.410	0.870	1.440
180°	1.090	1.620	2.820	3.370	2.940	1.260	1.440
225°	1.090	1.370	2.530	2.890	2.410	0.940	1.440
255°	1.090	1.200	2.140	2.650	2.050	0.850	1.440
270°	1.090	1.250	2.220	2.600	2.070	1.420	1.440
285°	1.090	1.560	2.750	3.140	2.740	1.730	1.440
315°	1.090	2.060	3.320	3.710	3.240	2.070	1.440
360°	1.090	2.370	3.510	3.830	3.560	2.350	1.440

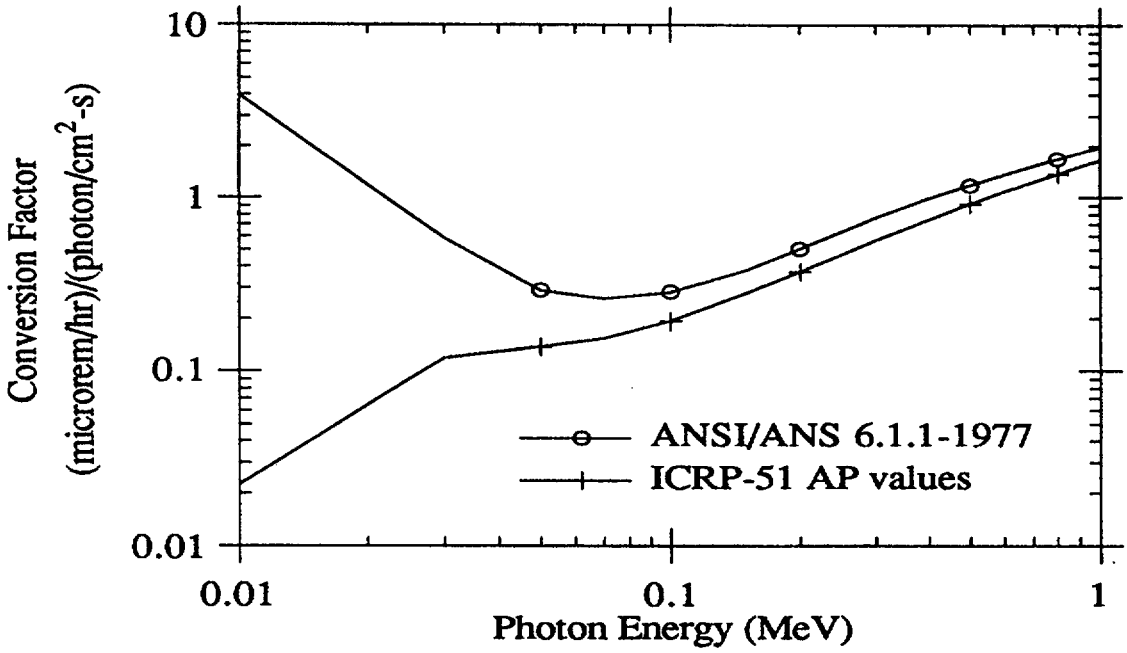

Figure 6. Flux-to-dose conversion factors

Questions have been raised as to the adequacy of dosimetry for nuclear power plant radiation workers, in particular, whether their dosimetry is at or near the point of highest exposure on the torso. Indeed, the NRC has cited some utilities for not having dosimeters at the point of highest external exposure. This concern has led to the widespread practice of multi-badging radiation workers and assigning the highest dose among the multiple dosimeters as the dose of record. This study shows that practice to be overly conservative. As the angle of beam incidence is changed from AP, effective dose equivalent drops dramatically. The decrease is often more than the angular under-response of a dosimeter;* thus, dosimeters will not generally under-predict H_E regardless of the incident photon angle. Moreover, dosimeters worn at the point of highest dose on the surface over-respond, since they are calibrated for AP exposures which produce the highest dose per unit fluence.

The beam data also demonstrate that dose assessment methodologies for external photons can be based on anthropomorphic phantoms rather than simple slabs, cylinders, or spheres as is often the practice. This will prevent overly conservative dose estimates, and establish dose estimates that realistically reflect the risk of radiation injury.

2.3 Point Source Results for Sources in Contact With the Torso

After completing the beam geometry study, doses from point sources were investigated. This geometry is the most difficult to characterize because effective dose equivalent is a function not only of source intensity, but also distance from the phantom. However, once H_E can be predicted for a point anywhere external to the phantom, then dose from all other simple sources can be calculated directly. A line source, for example, would be computationally divided into sections small enough to be approximated by point sources, and the effects of all sections summed to calculate the total dose from the line. Plane and disk sources can be handled in much the same way.

Effective dose equivalent from hundreds of point sources was calculated for photon energies of 0.08, 0.3, and 1.0 MeV. Source geometries considered started

* Dosimeters inherently respond less to radiation incident from the side than from the front.

with points in contact with the phantom torso, and moved outward to points three meters from the coordinate system origin. A diagram of the coordinate system used in MCNP to describe the phantom and the surrounding space is shown in Figure 7. The phantom is centered on the z-axis facing the negative y direction. Thus, points in space with negative y-coordinate values are in front of the phantom, while those with positive y-coordinate values are to the rear.

Because the phantom torso is mathematically described by an equation for a right elliptical cylinder, the surface can be flattened into two dimensions without distortion. The reader can imagine the torso surface being cut along the right side, then folded open and flattened out. (The process would be analogous to cutting a can down its side, bending the can open, and then flattening it.) With the torso so flattened it is easy to visualize how dose versus location on the torso can be mapped in two dimensions. Tables 5 through 7 list effective dose equivalent as a function of gender, photon energy, and position of the source on the torso. Location on the torso is expressed as height above the Z = 0 data plane (where the torso joins the legs) and distance around the torso (starting at the right side, continuing across the front to the left side, then continuing around the rear and terminating back at the right side).

For all photon energies, the highest effective dose equivalents for point sources in contact with the female torso occurs when the point source is on the front of the torso near the sternum. For males it occurs when the source is on the front of the torso near the gonads.* For all photon energies, effective dose equivalent from a point source on the male gonads is higher than effective dose equivalent from an identical source on the sternum of the female. However, for all other point source locations, the female has a higher effective dose equivalent per unit exposure than the male.

* The breasts are the most radio-sensitive organs in the female. The gonads are the most radio-sensitive organs in the male and the second most radio-sensitive in the female. See Table 1.

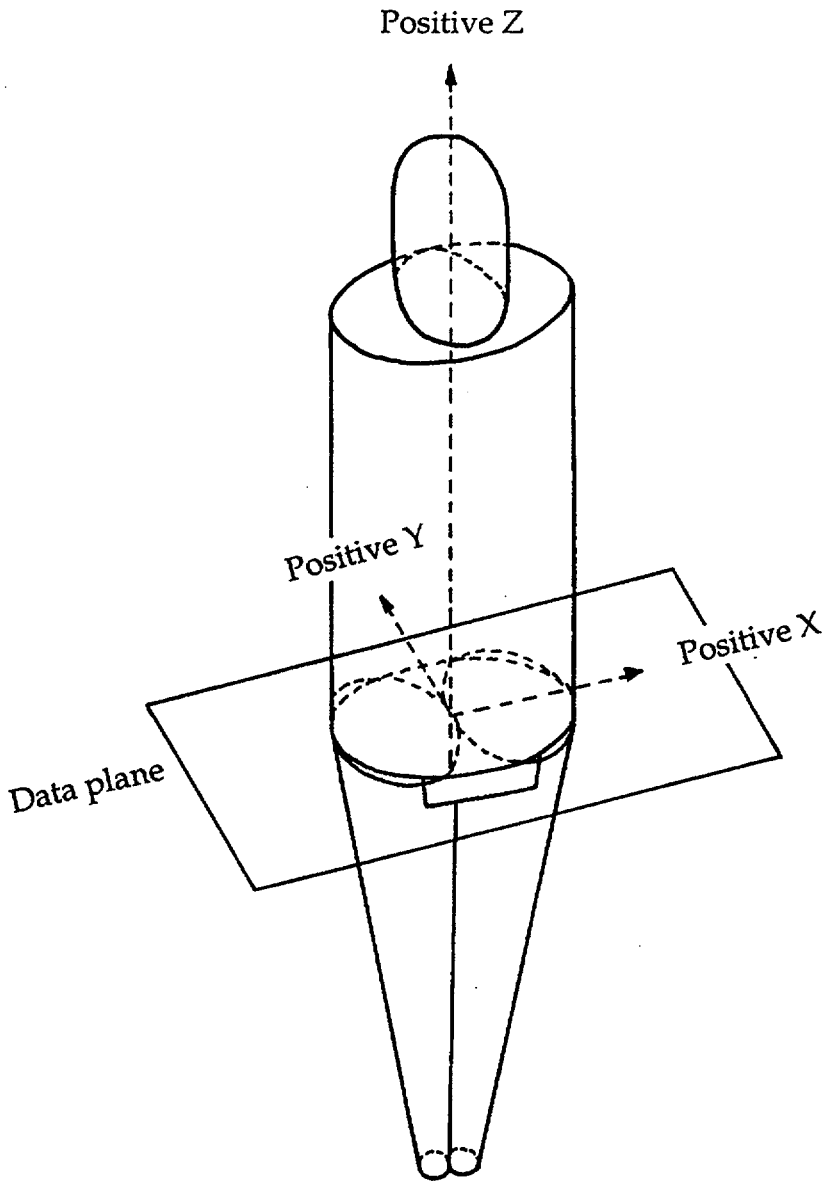

Figure 7. Schematic of the phantom coordinate system

Table 5. Effective Dose Equivalent as a Function of Point Source Location on the Torso (0.08 MeV Photons, units = rem per photon x E-15)

Adult Female

Distance From "Cut" (cm)*	Location on the Torso	Height Above Data Plane (cm)** 6	21	41	61
0.00	right side	1.56	2.49	2.76	2.10
5.15		2.54	4.58	5.93	5.44
15.03		5.35	8.89	10.88	11.74
25.30	front	9.19	9.60	11.48	15.21
35.56		5.88	7.95	12.28	11.65
45.44		2.75	4.08	6.76	5.40
50.59	left side	1.56	2.36	3.45	2.09
55.74		2.54	3.42	5.53	2.94
65.62		4.57	6.62	9.45	4.52
75.89	back	5.20	8.96	10.39	5.12
86.15		4.23	6.82	7.53	4.51
96.03		2.28	3.52	3.91	2.99
101.18	right side	1.56	2.49	2.76	2.10

Adult Male

Distance From "Cut" (cm)*	Location on the Torso	Height Above Data Plane (cm)** 6	21	41	61
0.00	right side	1.15	1.72	2.22	1.50
5.15		1.81	2.85	3.32	2.18
15.03		5.72	5.68	5.70	4.29
25.30	front	14.29	5.36	6.98	9.62
35.56		6.15	4.61	7.07	4.22
45.44		2.08	2.46	4.17	2.15
50.59	left side	1.15	1.59	2.90	1.48
55.74		1.74	2.29	5.07	2.50
65.62		2.93	4.19	8.81	3.87
75.89	back	3.01	5.91	9.86	4.63
86.15		2.49	4.33	6.80	3.85
96.03		1.45	2.38	3.43	2.53
101.18	right side	1.15	1.72	2.22	1.50

* The distance from the simulated "cut" along the right side of the torso (see text).

** The plane where the bottom of the torso meets the top of the legs (see Figure 7).

Table 6. Effective Dose Equivalent as a Function of Point Source Location on the Torso (0.3 MeV Photons, units = rem per photon x E-15)

Adult Female

Distance From "Cut" (cm)*	Location on the Torso	Height Above Data Plane (cm)** 6	21	41	61
0.00	right side	6.96	10.77	12.52	9.42
5.15		9.77	17.27	23.13	20.95
15.03		19.18	31.77	40.13	43.83
25.30	front	32.21	33.35	42.85	56.34
35.56		20.40	28.53	45.12	43.62
45.44		10.94	16.22	26.01	20.89
50.59	left side	6.96	10.33	15.15	9.50
55.74		9.69	13.33	20.93	10.88
65.62		16.22	23.08	34.04	15.51
75.89	back	18.19	29.04	36.27	16.28
86.15		14.68	23.59	27.19	15.35
96.03		8.80	13.68	15.35	10.87
101.18	right side	6.96	10.77	12.52	9.42

Adult Male

Distance From "Cut" (cm)*	Location on the Torso	Height Above Data Plane (cm)** 6	21	41	61
0.00	right side	5.04	7.13	9.21	5.87
5.15		7.48	10.58	12.27	7.75
15.03		22.16	19.97	19.76	14.62
25.30	front	52.04	19.14	24.15	33.94
35.56		22.93	16.62	24.46	14.53
45.44		8.30	9.41	15.03	7.65
50.59	left side	5.04	6.65	11.78	5.87
55.74		6.64	8.63	18.34	8.44
65.62		10.29	13.71	30.33	12.21
75.89	back	10.81	17.80	33.04	13.44
86.15		8.60	14.18	23.49	12.04
96.03		5.63	8.84	12.69	8.39
101.18	right side	5.04	7.13	9.21	5.87

* The distance from the simulated "cut" along the right side of the torso (see text).

** The plane where the bottom of the torso meets the top of the legs (see Figure 7).

Table 7. Effective Dose Equivalent as a Function of Point Source Location on the Torso (1.0 MeV Photons, units = rem per photon x E-15)

Adult Female

Distance From "Cut" (cm)*	Location on the Torso	Height Above Data Plane (cm)** 6	21	41	61
0.00	right side	26.43	41.71	49.49	37.82
5.15		36.75	60.29	78.24	70.07
15.03		64.17	103.50	129.80	140.40
25.30	front	103.90	109.20	137.80	179.00
35.56		68.29	93.64	144.50	140.40
45.44		38.91	57.06	87.24	70.04
50.59	left side	26.43	40.11	57.98	37.88
55.74		35.24	48.95	73.77	41.15
65.62		53.59	77.90	112.70	53.52
75.89	back	60.71	95.33	120.10	57.57
86.15		51.06	78.52	91.57	53.00
96.03		32.10	49.34	59.39	40.90
101.18	right side	26.43	41.71	49.49	37.82

Adult Male

Distance From "Cut" (cm)*	Location on the Torso	Height Above Data Plane (cm)** 6	21	41	61
0.00	right side	20.83	27.82	34.26	22.56
5.15		29.11	38.66	42.56	27.64
15.03		75.75	67.22	65.02	48.91
25.30	front	168.50	65.31	79.20	109.10
35.56		77.36	57.16	79.38	48.92
45.44		31.56	34.61	51.53	27.52
50.59	left side	20.83	26.27	42.95	22.46
55.74		25.82	31.94	62.35	29.98
65.62		36.17	47.16	98.42	40.92
75.89	back	38.40	59.77	106.40	45.40
86.15		31.57	48.28	77.05	40.38
96.03		22.53	32.52	44.23	29.68
101.18	right side	20.83	27.82	34.26	22.56

* The distance from the simulated "cut" along the right side of the torso (see text).

** The plane where the bottom of the torso meets the top of the legs (see Figure 7).

2.4 Point Source Results for Sources Away From the Torso

Doses from point sources three meters or more away from the phantom can be predicted using beam geometry results. As point sources are moved further away from the phantom, photons from these sources arrive ever more parallel, asymptotically approaching beam geometry. The intensity of a point source far from the phantom is proportional to the square of the distance between the source and the phantom:

$$\text{intensity } [\text{photons/cm}^2] = \text{photons emitted} / 4\,\pi\,\text{distance}^2 \qquad \text{Eq. 2}$$

As discussed in reference 2, various values might be used for the "distance" term in the above equation. It could be the closest distance to the phantom or the distance from the center of the coordinate system. As the point source distance increases, the difference in distance between the closest location on the torso and the center of the coordinate system becomes a small fraction of the overall distance, and has little influence on the calculation. Using the geometric mean of the two distances provides a good solution. For point sources farther than three meters from the surface of the phantom, Equation 2 calculates effective dose equivalent with an error less than 10%.

Sources located between contact and three meters are quite interesting to characterize. Figure 8 shows three-dimensional projections of H_E versus point source location for a female exposed to a 1.0 MeV point source. The source is at a constant height—6, 41, or 61 cm—above the plane of the coordinate system (dividing the torso and the legs of the phantom). Figure 9 shows a similar plot for males. Though the structure of the data plots appear complicated, the features are generally understood. By carefully considering the location and geometry of the radiation sources, the anatomical features of the phantom, and the relative weighting factors of the organs exposed, the three- dimensional structure can be explained. Though the photon interactions with the body are complex, organ dose and effective dose equivalent can be readily calculated.

In summary, for the same photon fluence on the torso, point sources are shown to be relatively innocuous compared to uniform exposure from beams. Flux from a point source decreases as the reciprocal of the distance from the source, squared.

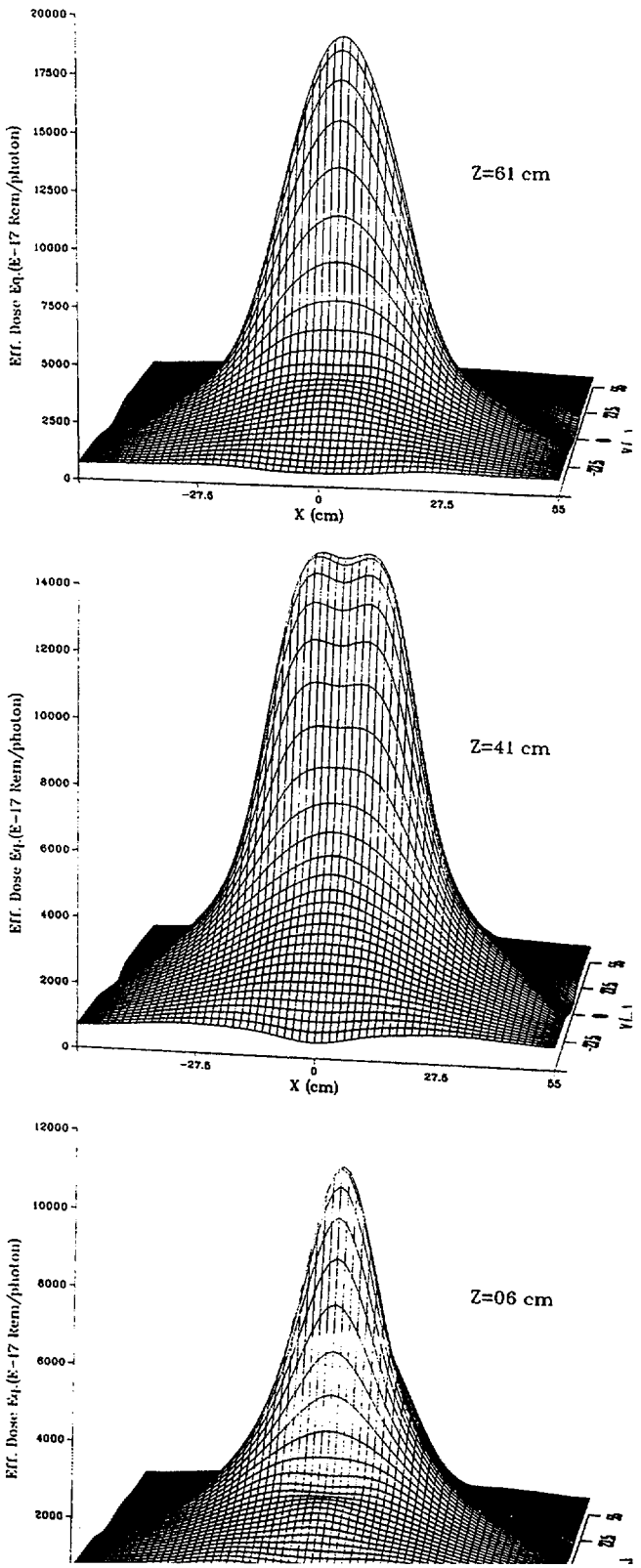

Figure 8. Surface plots of H_E for a female vs. source location for a 1.0 MeV point source

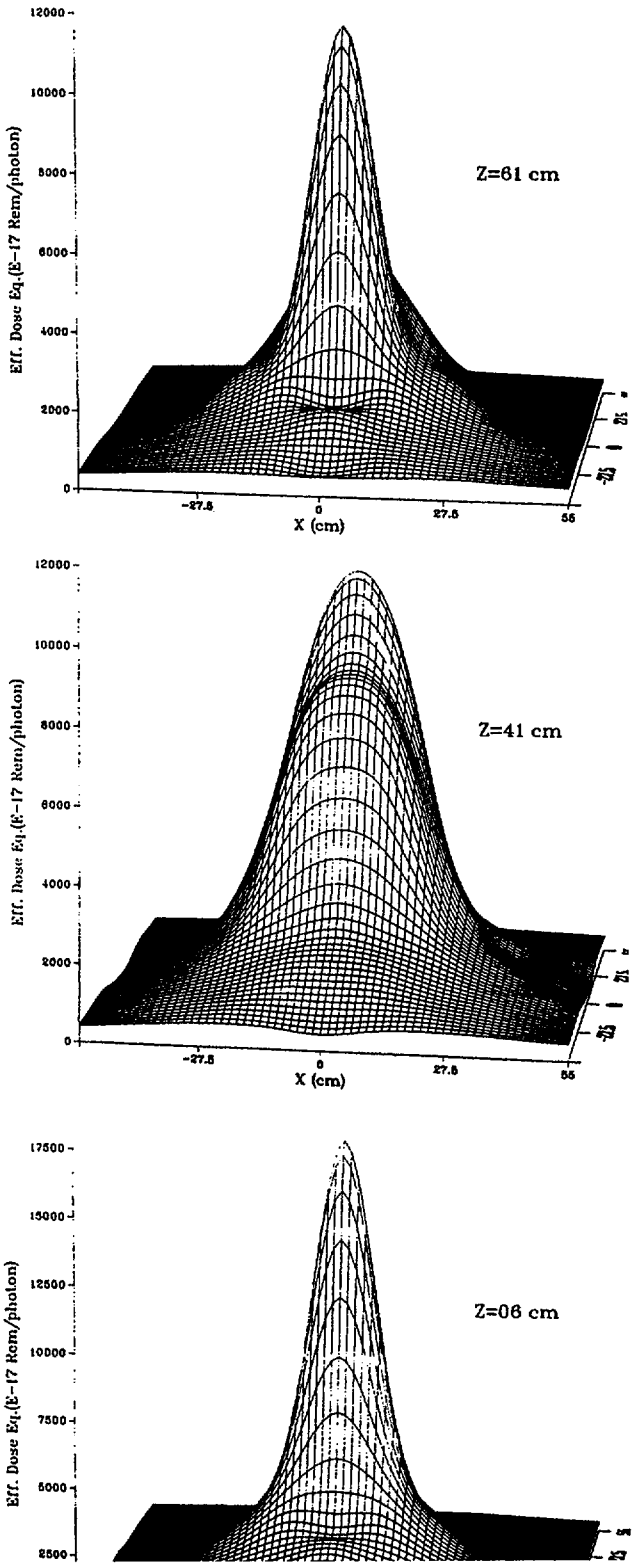

Figure 9. Surface plots of H_E for a male vs. source location for a 1.0 MeV point source

Point sources near the torso generate small doses for organs and tissues proximal to the source because of this rapid decrease in flux. This is true even if shielding by intervening tissues is ignored. The effective dose equivalent drops orders of magnitude for sources a foot or more away from contact with the torso.

This section is an abbreviated summary of the Volume 1 results. Additional tabular and graphical data and further discussion and interpretation of effective dose equivalent from beam and point sources will be found in Volume 1 (reference 2).

3.0 PHOTON ENERGY FLUENCE CALCULATIONS FOR BEAM AND POINT SOURCES

3.1 Overview

In the first phase of this study—summarized in Section 2—we calculated effective dose equivalent for male and female workers exposed to ionizing radiation from beam and point sources for a range of photon energies typical of those encountered at nuclear power plants. As a result of these calculations we now understand how radiation striking the body from any direction interacts with various organs and tissues. We also understand the relative risk because we understand the radiation dose to all the organs and tissues, as well as the summation of those organ doses (the effective dose equivalent).

To make practical use of effective dose equivalent calculations, however, we need additional data. We cannot place dosimeters in organs, nor can we know in detail the energy, geometry, and exposure time of all sources encountered when performing a task in a radiation field. Radiation workers wear external dosimeters, typically on the outside of their protective clothing, which provides a measure of total photon energy fluence at discrete locations on the surface of the body. Thus, the next step in relating dosimeter readings to effective dose equivalent is to understand—for beam and point sources—how photon energy fluence varies as a function of location on the surface of the body.

3.2 Calculational Approach

NRC regulations require workers who are likely to receive an effective dose equivalent exceeding 10% of the limit to wear a monitoring device (a personnel dosimeter). Typically a single dosimeter is attached to a worker's protective clothing at the chest or waist level. The dosimeter reading, upon proper calibration, is used to determine the dose of record for the wearer. The challenge is to relate the dosimeter reading to the worker's actual effective dose equivalent within a certain confidence level. The principles of radiation dosimetry, including uncertainties and errors in measurement, have been discussed in detail in ICRP Publication 35.[7] It is important to remember that the quantity measured by a dosimeter is not the quantity on which regulatory limits are based

(effective dose equivalent). Also, the response of dosimeters is influenced by factors such as the dosimeter location and orientation of the worker's body in the radiation field (the body may partially shield the dosimeter). Thus, correlating external dosimeter readings to effective dose equivalent received by internal organs is a complex task.

One goal of this research was to study the relationship between dosimeter response when worn at various locations on the body, and effective dose equivalent as determined by Monte Carlo calculations for a human phantom as described above. To understand how dosimeter positioning affects dosimeter readings, personnel dosimeters were simulated at many locations on the surface of the phantom. Photon energy fluences were calculated at these locations. A simplified adult phantom, which did not model all internal organs, was deemed adequate for this phase of the study. The skeleton was modeled because bone structure is a shield and backscatters photons, and the lungs were modeled because of their high transparency to photons. The simplified phantom was hermaphroditic, that is it was modeled with female breasts and male gonads. The breasts, gonads, and all other structures were modeled as uniform body tissue.

To simulate dosimeters, the size, geometric shape, and material of the dosimeter generally needs to be specified in MCNP. Many researchers have simulated dosimeters in Monte Carlo calculations.[8,9] In most cases, dosimeters are modeled as simple shapes (spheres or cubes) of tissue-equivalent material. Typically only one or a few dosimeters are modeled on the surface of a phantom. In this study dosimeter simulations were performed differently. Small air-filled spheres, each with a radius of 1 cm, were defined at 480 different locations on the surface of the phantom, including the head, torso, left upper leg, and right upper leg. (A list of dosimeter locations is given in reference 10.)

There are several advantages to modeling air spheres on the surface of the phantom rather than modeling an actual dosimeter.

- Air spheres do not alter photon transport or scattering properties on the surface of the phantom as other media would.

- The influence of dosimeter position on dosimeter reading can be easily studied by investigating many different dosimeter locations in the same MCNP computer run. This is because the phantom is surrounded by air, and our dosimeters (mathematically defined air-filled spheres) do not change the composition of the surroundings at the surface of the phantom. Since each dosimeter is merely an air-filled space, no dosimeter has a computational influence on its neighbors.

- Specifying the design, construction, and material of a physical dosimeter can be avoided. A physical dosimeter may be too complicated to be modeled exactly, and a particular manufacturer's dosimeter need not be specified.

- Dosimeter readings for different types of dosimeters can be obtained later by applying the mass energy-absorption coefficients for actual dosimeter materials.

The disadvantage of this approach is that actual dose—as measured by a thermoluminscent chip located within the dosimeter—will be smaller than calculated due to attenuation in the plastic dosimeter holder (though this is easily corrected). More important, because of the shields over the TLD and the physical construction of the dosimeter package, most dosimeters respond differently depending upon the incident photon angle. Nonetheless, modeling air-filled spheres is a good starting point for evaluating dosimeter response, and correction factors can be subsequently applied to account for attenuation, angular response, or other factors.

For both beam and point sources and for a range of photon energies, the MCNP code tallied the number of photons entering each sphere as well as the track length of each photon contained within the spherical volume. The code tracked photons directly incident on the sphere as well as photons backscattered from inside the body into the spherical volume. This method is quite reliable because a large number of tracks were tallied in each sphere.

Height along the body was expressed as Z-axis values, with the juncture of the phantom's torso and legs at Z = 0 cm (see Figure 7). Dosimeter locations were defined on each region of the phantom:

- head: Z = 71 to 91 cm
- torso: Z = 1 to 66 cm
- upper legs: Z = -4 to -49 cm.

Figure 10 shows a cross section of the phantom at slightly above mid-torso (Z = 41 cm).* The dosimeter locations (air-filled spheres) are apparent on the torso's surface. The 480 dosimeter locations on the phantom were selected not only to account for the most common dosimeter placements found in nuclear power plant operations, but also for special operations when dosimeters are sometimes placed on top of the head, the upper legs, and the front, lateral, or back side of the body to account for highly directional radiation sources. Calculations at such a large number of locations allows dosimeter response to be expressed as contour lines on the surface of the phantom.

Once the photon number and track length tallies were completed for a dosimeter location, the dose to an "ideal" dosimeter could be calculated. The photon energy fluence is multiplied by the mass-energy absorption coefficient, μ_{en}, to convert photon track length estimates of the fluence to dose. These coefficients are proportional to the fraction of the photon beam energy deposited locally around the dose point. The mass-energy absorption coefficients depend on the material absorbing the energy and the energy of the photons. We used mass-energy absorption coefficients provided by Hubbell[11] and tabulated as a function of energy and material by Attix.[12] Thus, to calculate dose to a dosimeter at a particular location, each tally from MCNP for a particular energy bin (tabulated at energies of 0.01, 0.02, 0.03, 0.04, 0.05, 0.06, 0.08, 0.10, 0.15, 0.20, 0.30, 0.40, 0.50, 0.60, 0.80, 1.0 MeV) is multiplied by the mass-energy absorption coefficient for the dosimeter material at the bin energy. By summing over all energy bins, the total dose at that location can be calculated.

Two implicit assumptions are made by calculating dose in this way. First, because photons are not charged, it is secondary electrons created by the photons that

* The breasts are not visible in this figure because this cross-section is just below their location.

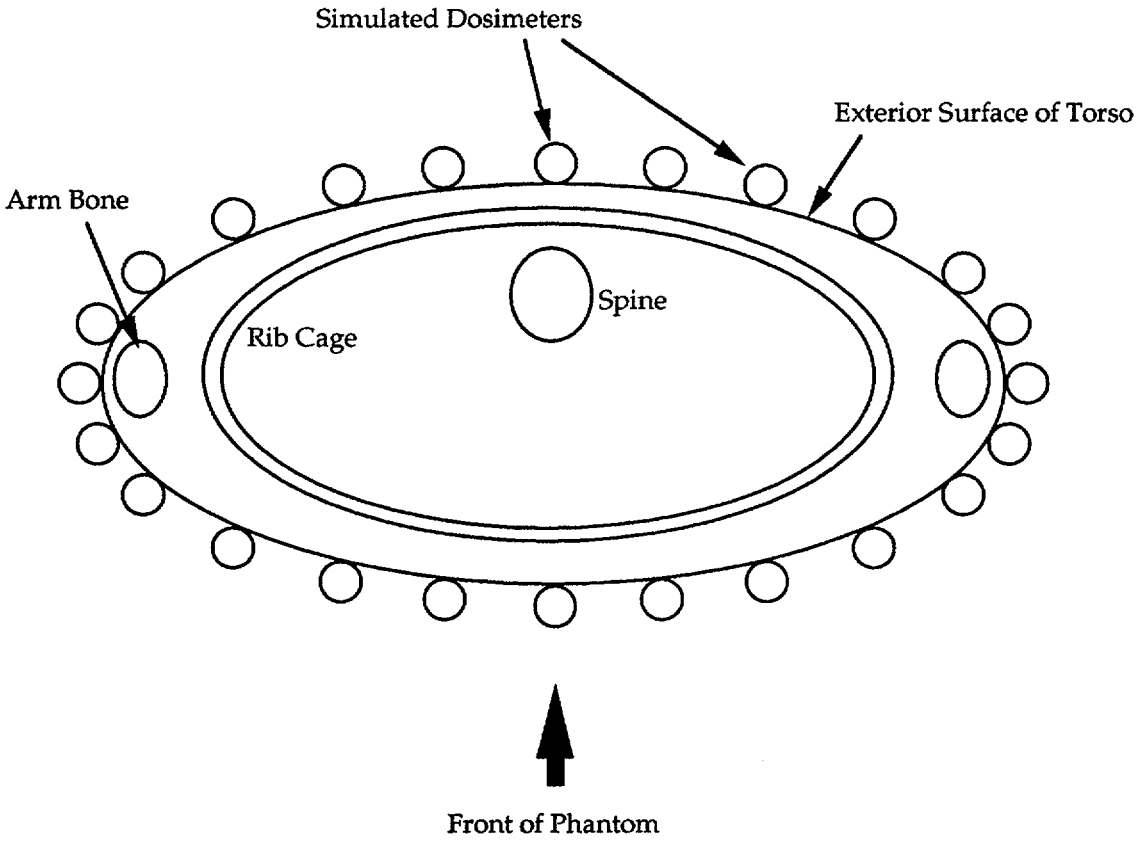

Figure 10. Cross section of the phantom at Z = 41 cm

deposit energy in the dosimeter. Going from photon energy fluence to dose is not strictly correct unless a condition called *charged particle equilibrium* exists. This topic is addressed in many texts on dosimetry (for example, Attix[12]), and fortunately for all present dosimeter designs this equilibrium condition exists. The second assumption is the concept of an "ideal" dosimeter. Ideal dosimeters are isotropic; they respond the same regardless of incident photon direction. This is not the case for most dosimeter packages used presently. We will discuss later how non-isotropic response of dosimeters can be advantageous when evaluating effective dose equivalent.

There are two important reasons for studying the influence of dosimeter position on dosimeter reading. First, we want to know whether one or more locations exist for optimum dosimeter placement. Second, if such locations exist we then can develop algorithms using dosimeters at those locations to accurately assess a worker's effective dose equivalent. Alternatively, if there is no significant difference in response for different dosimeter locations, we may select a conventional dosimeter location—such as on the chest or waist—and recommend algorithms without any specific requirements for dosimeter placement.

For our dosimeter simulations the hermaphroditic phantom with small air-filled spheres on the surface was "irradiated" (using the MCNP code) by broad parallel photon beams of various energies. We also investigated isotropic point sources. While we did not investigate a wide range of sources, we did examine point sources close to the body (such as might be encountered by workers doing maintenance or other "hands on" tasks). Accordingly—as discussed in Section 4—when we evaluated the ability of various dosimeter algorithms to accurately assess effective dose equivalent for beams, we extended the evaluations to a representative sampling of point sources.

For broad, parallel, photon beam sources, surface energy fluence and dosimeter response were calculated for the five irradiation geometries used for effective dose equivalent calculations: AP, PA, LAT, overhead, and underfoot. In addition, photon beams incident from azimuthal and polar angles of 45° were used to represent an arbitrary irradiation geometry. These results were used to assess how dosimeters at various locations correlate with effective dose

equivalent, and for evaluating various dosimeter algorithms. Due to the large number of simulated dosimeters and the variety of energy and geometries involved, the dosimeter simulation results are not easily presented in tables. Thus, to present the results graphically, the entire phantom (head, torso, and upper legs) was "cut" along the back, folded open and flattened into two-dimensions. The energy fluence calculations were then plotted as contour lines on this representation of the phantom.

3.3 Results for Dosimeter Simulations

Figure 11 presents dosimeter response contour plots for AP photon beams (incident from the front) for 0.08, 0.3, and 1.0 MeV photons. (These are the same energies used for effective dose equivalent evaluations.) Similarly, results for the PA (incident from the back), LAT (incident from the side), overhead, underfoot, and the arbitrary geometry (45° azimuthal and 45° polar) are presented in Figures 12 through 16. Spline interpolations were performed in order to draw smooth contour lines among the data obtained from the 480 air spheres on the surface of the phantom. The reading for the dosimeter located at about mid-torso (Z = 41 cm) on the front of the phantom was used to normalize the results, and this reference numerical value (called the dosimeter kerma unit) is given at the top of each figure in units of Sv per photon fluence (Sv/cm^2). Data shown on the contour lines are the relative dosimeter response at that location, and can be multiplied by the reference numerical value to obtain the absolute dosimeter response.

Inspection of these figures shows, for all energies and geometries, dosimeter responses can be classified into two distinct groups:

1. dosimeters located close to each other with responses that are almost equal
2. dosimeters located close to each other but with responses with large variations.

Dosimeters with almost the same responses are located on the side of the phantom facing the radiation beams, and can therefore "see" the source directly. While dosimeters with large variations are located on the opposite side of the phantom as the source, and are partly shielded by the phantom. Clearly, dosimeter response is influenced by both dosimeter placement and the worker's orientation in the radiation field, as discussed in more detail below.

(this page is intentionally blank)

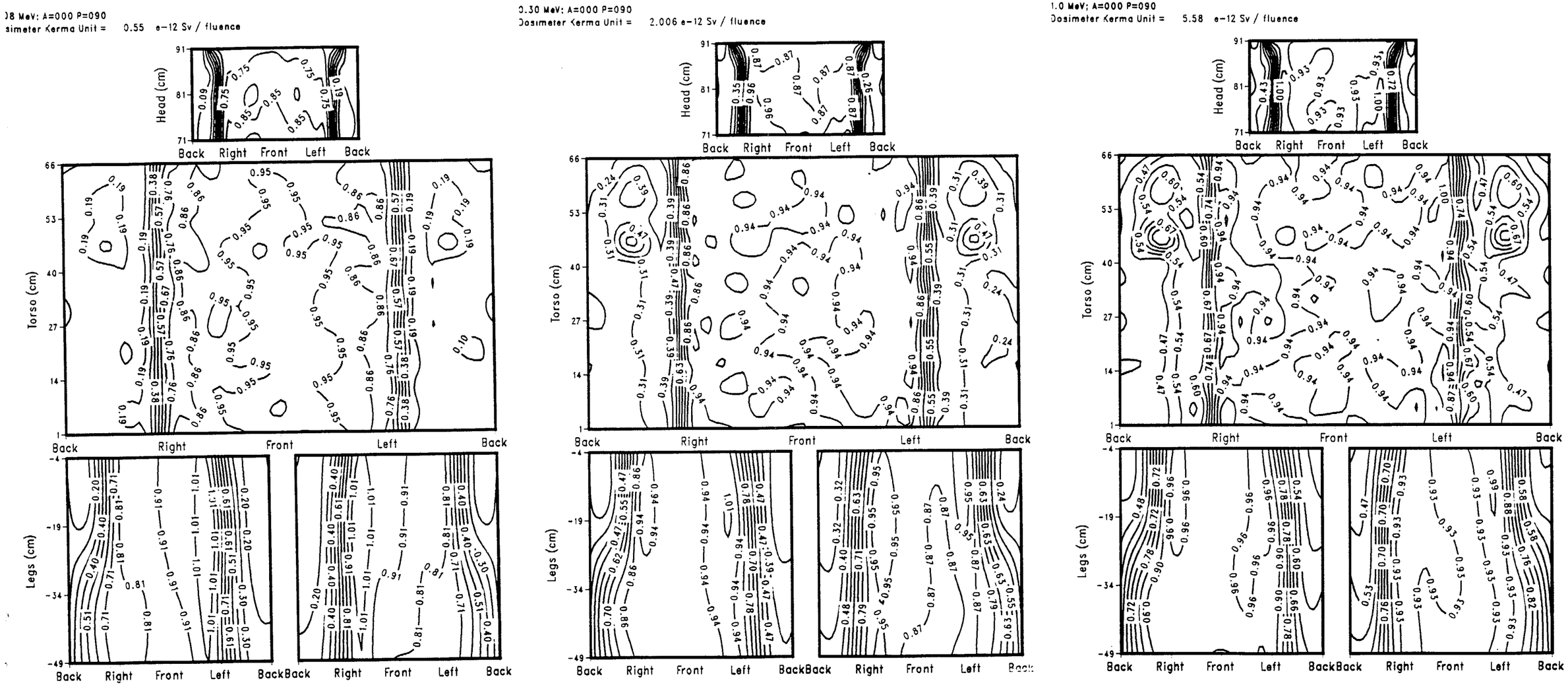

Figure 11. Contour plot of normalized dosimeter response for phantom exposed to AP beam source.

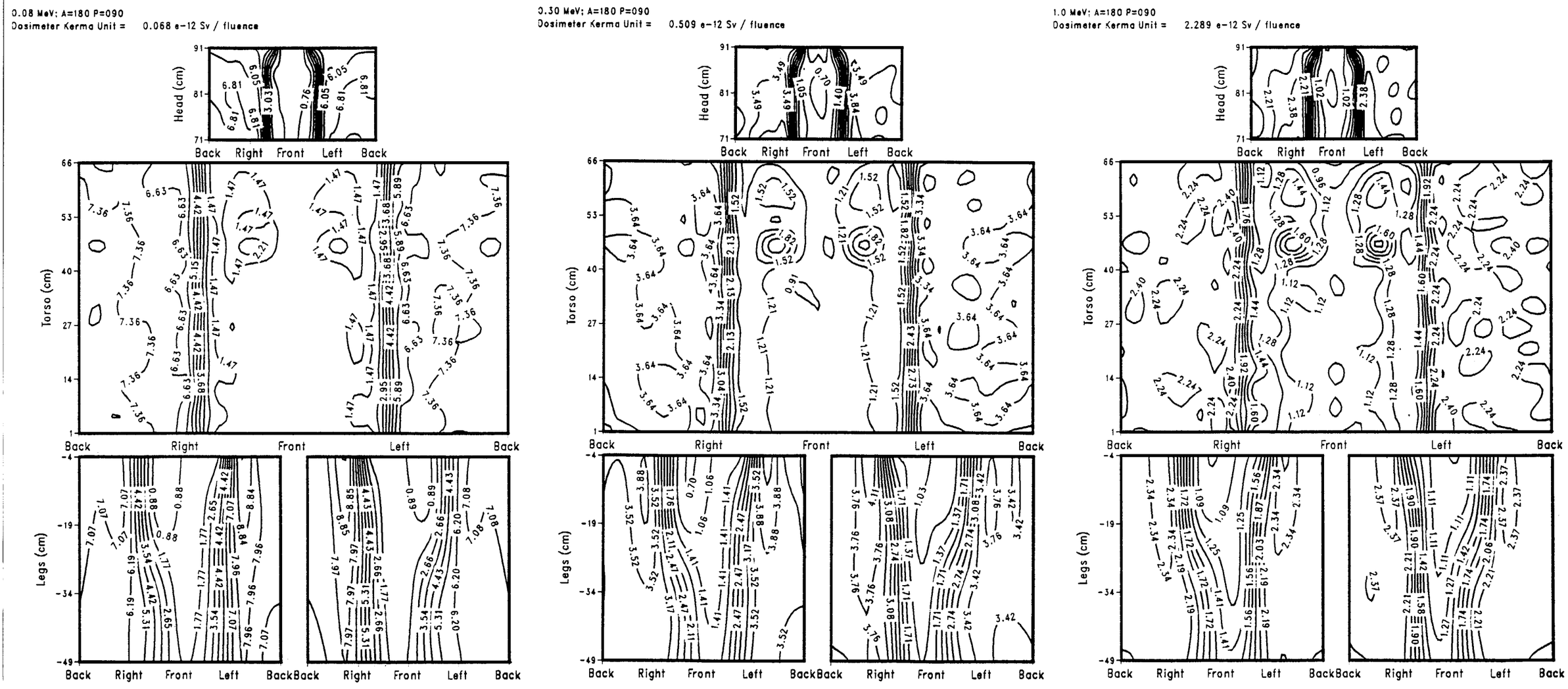

Figure 12. Contour plot of normalized dosimeter response for phantom exposed to PA beam source.

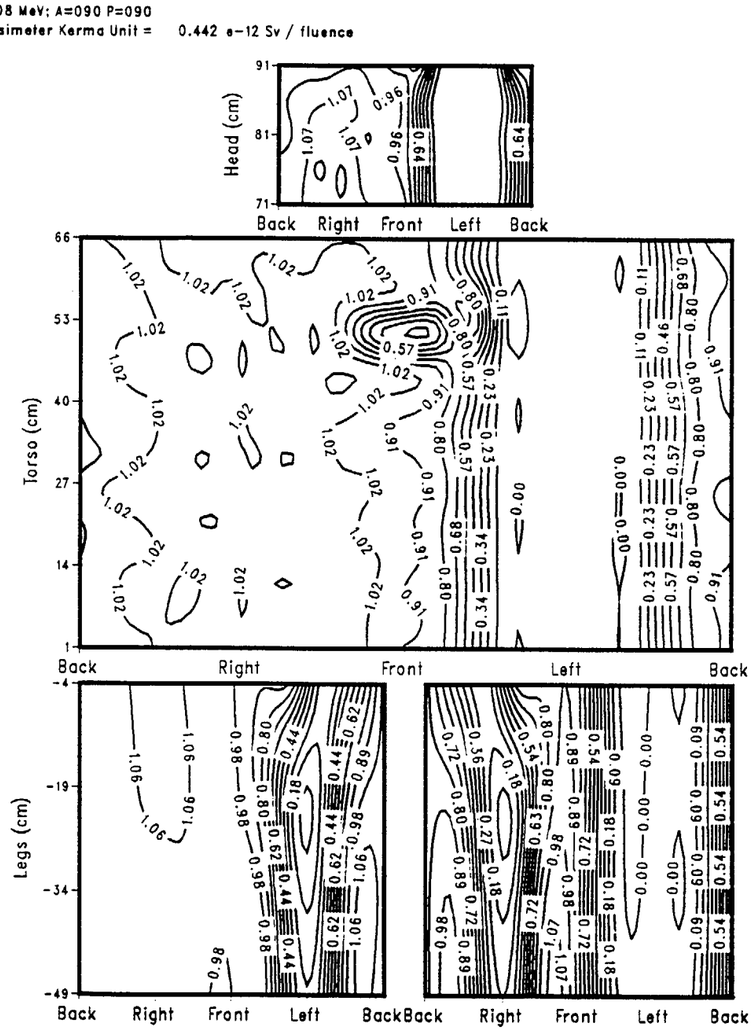

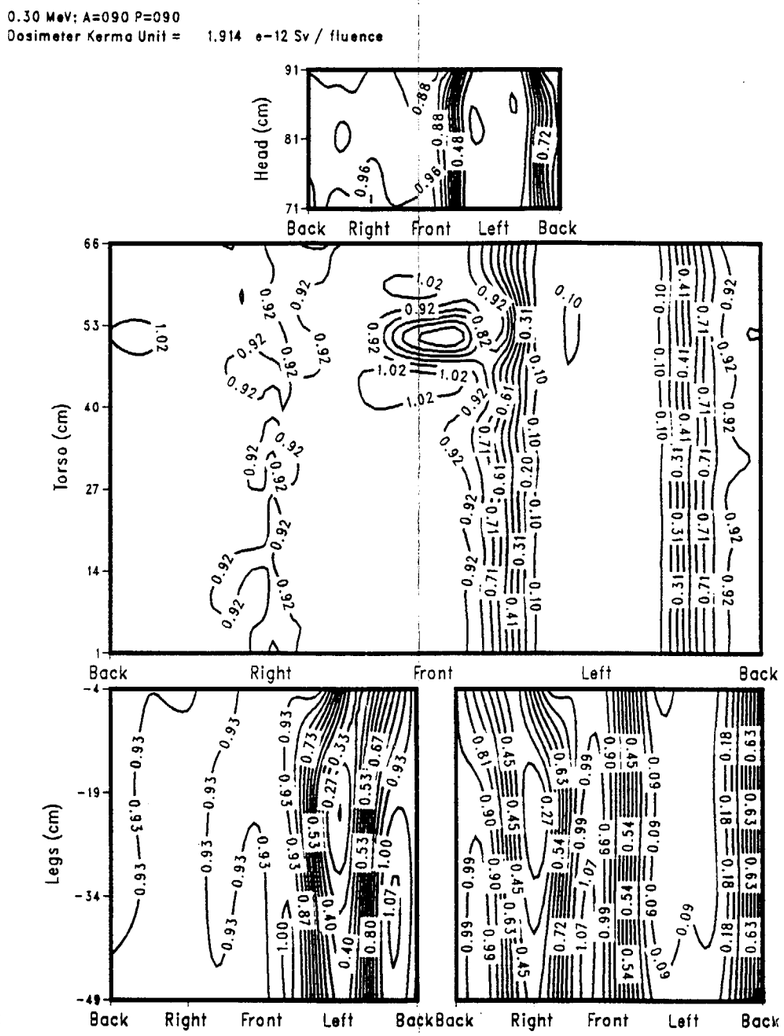

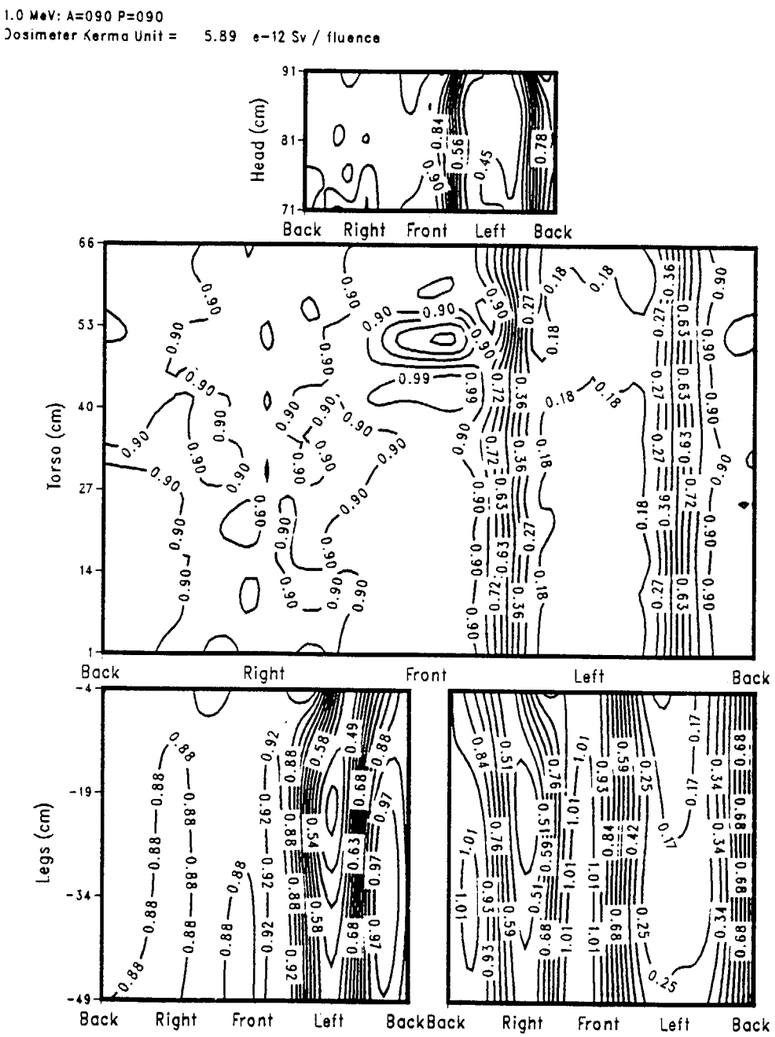

Figure 13. Contour plot of normalized dosimeter response for phantom exposed to LAT beam source.

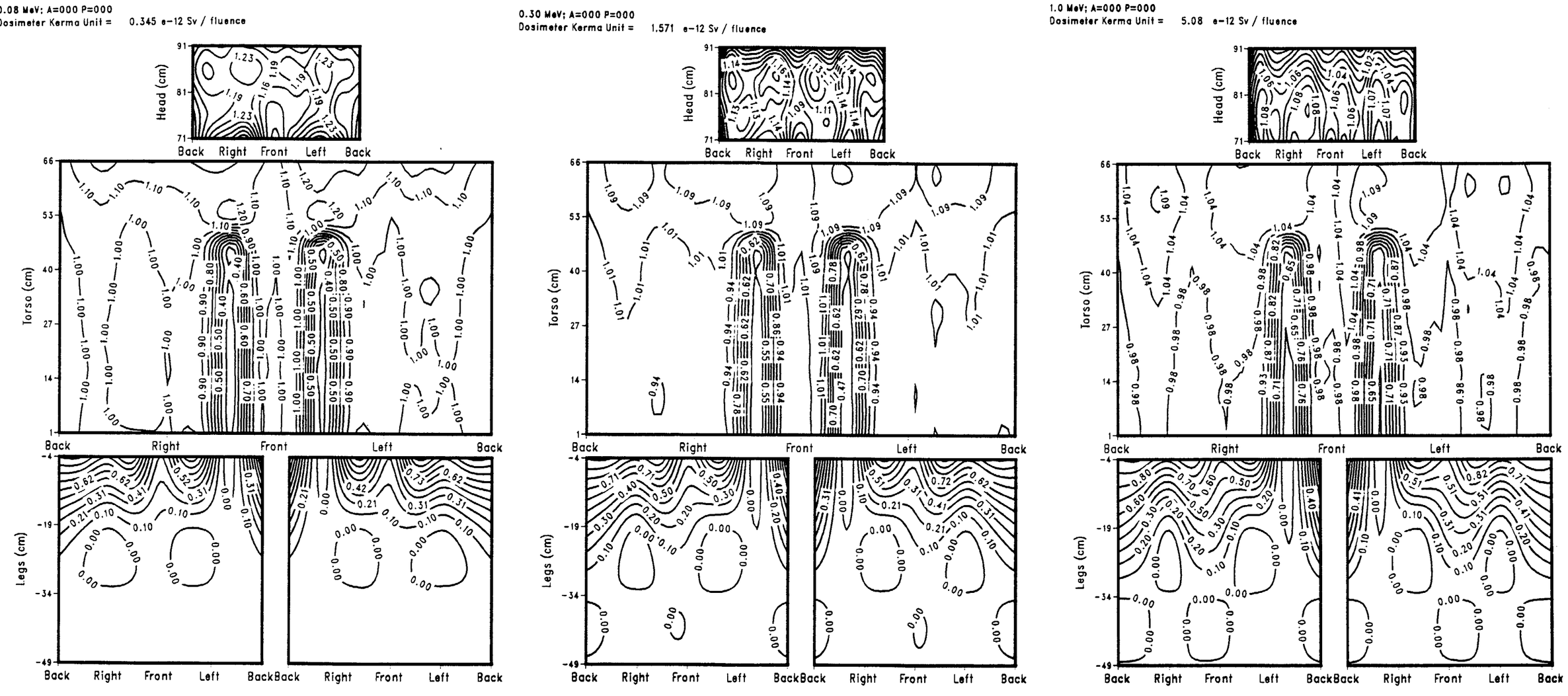

Figure 14. Contour plot of normalized dosimeter response for phantom exposed to Overhead beam source.

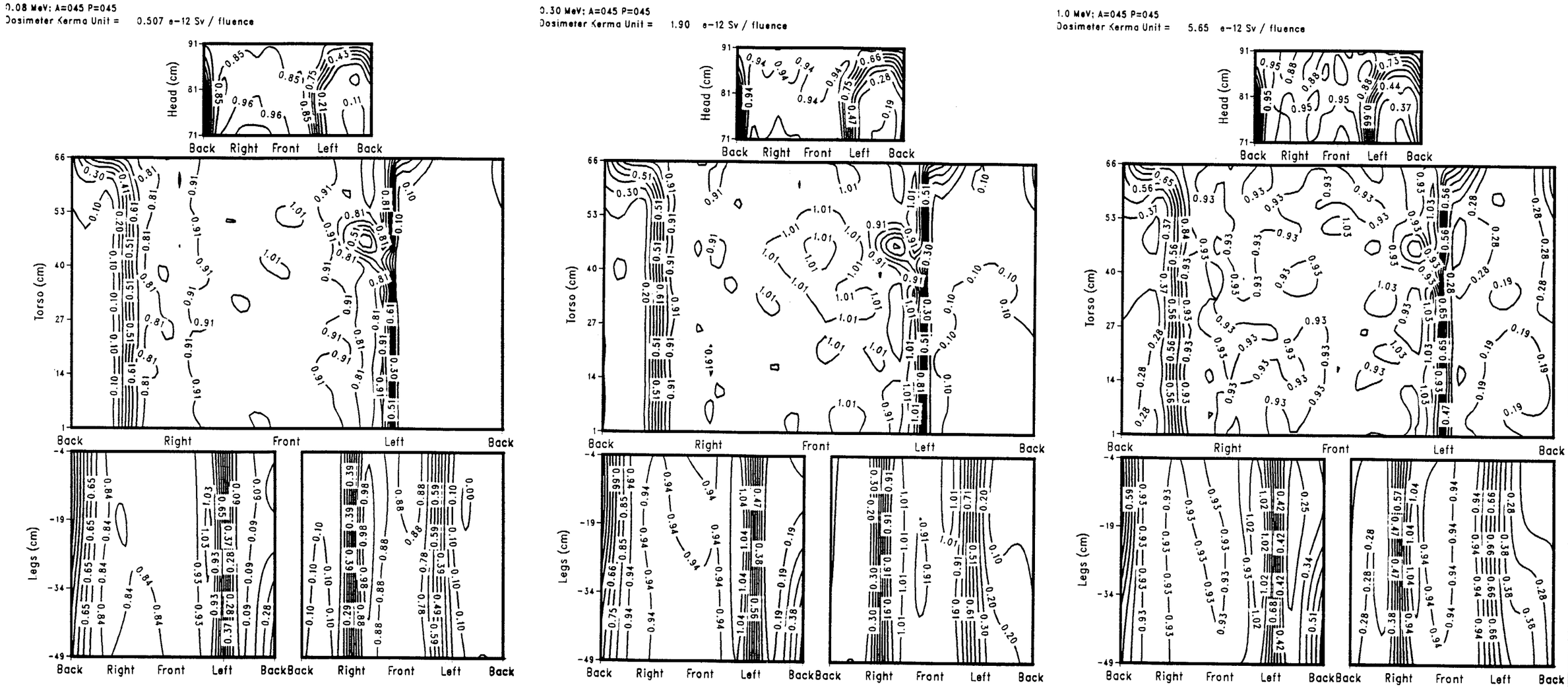

Figure 16. Contour plot of normalized dosimeter response for phantom exposed to Arbitary beam source (A= 45° and P=45°)

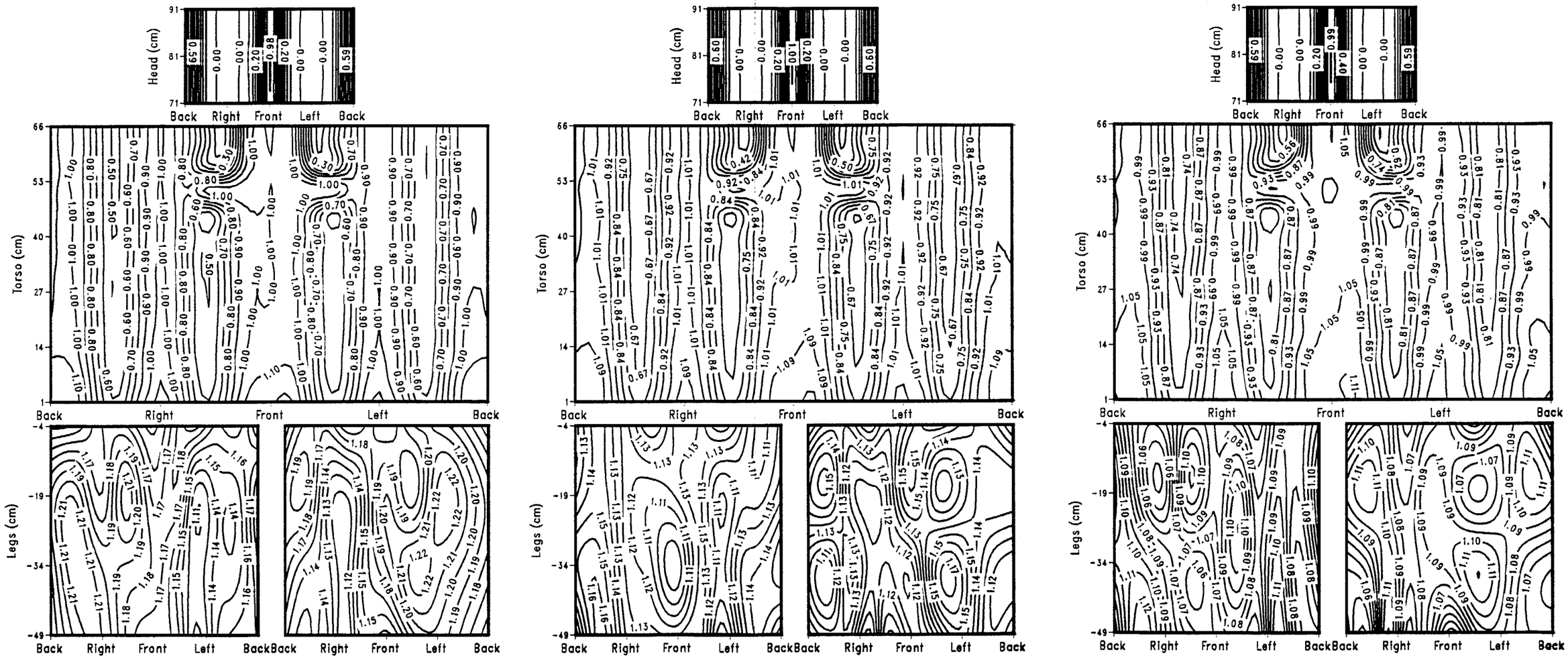

Figure 15. Contour plot of normalized dosimeter response for phantom exposed to Underfoot beam source.

(this page is intentionally blank)

3.3.1 AP Exposures

AP photon beams strike the body from the front at right angles to the body's long axis. Figure 11 shows contour plots of normalized dosimeter response for this geometry for the three photon energies studied. Dosimeters facing the radiation source are in the regions of the phantom labeled "Front" and extending in either direction to the areas labeled "Right" and "Left." The normalized readings for these front-facing dosimeters vary somewhat depending on photon energy and location on the phantom, but generally range from about 0.85 to 1.0. For dosimeters located on the very front of the torso from the chest to the hips, the readings are practically the same (ranging from about 0.94 to 1.0). Since the incident fluence for AP exposures is the same for all dosimeters placed on the front of the body, the differences result solely from variations in photon backscatter at different locations on the body's surface. Most backscattered photons have low energies and their contribution to the dosimeter response is small. These results suggest that for whole body AP exposures—probably the most common exposure encountered in the workplace—a specific requirement on dosimeter location is not necessary, provided the dosimeter directly "sees" the source. Therefore, dosimeters worn on the forehead, thorax, abdomen, or front of the upper legs, will exhibit almost the same readings.

As expected, dosimeters worn on locations on the body shielded from AP beams (the regions labeled "Back" to "Right" and "Left" to "Back" in Figure 11) show much larger variations in dosimeter response, and these variations are influenced by photon energy. The relative response for these "shielded" dosimeters varies as follows:

- 0.08 MeV photons: ~ 0.1 to 0.75
- 0.3 MeV photons: ~ 0.25 to 0.85
- 1.0 MeV photons: ~ 0.45 to 0.90.

The large variations in response are caused by the variations in tissue densities. Low-density tissue such as the lungs allows more photons to penetrate the body and reach "shadowed" dosimeters, while bones cause significant attenuation and backscattering. The maximum response difference among partially shielded dosimeters is greater, of course, for less penetrating photon beams.

Nonetheless, dosimeters shadowed by the body still indicate, to some degree, the total radiation to which the body is exposed. A dosimeter located on the upper back (at Z = 41 cm) reads about 10% of the value of a dosimeter at the same height on the chest for 0.08 MeV photons for AP exposures. These relative readings increase to about 25% and 45% respectively for 0.3, and 1.0 MeV photon beams. As discussed below, these relative readings can help to reconstruct effective dose equivalent exposures for situations of unknown geometry, or when workers are moving relative to radiation sources.

3.3.2 PA Exposures

PA photon beams strike the body from the back at right angles to the body's long axis. Figure 12 shows contour plots of normalized dosimeter response for this geometry for the three photon energies studied. Readings are normalized to a dosimeter worn at the center of the chest, which is a "shadowed" dosimeter in this geometry. Thus, the numerical values of the contour lines on the back of the phantom are much greater in these figures. Keeping this difference in mind, PA geometry results are similar to AP geometry. That is, a dosimeter placed anywhere on the back of the phantom (the head, torso, or back of the upper legs) will produce almost the same response for radiation incident from the rear-half plane of the body. Dosimeters shielded by the body show larger variations, as they do for AP geometry.

As shown in Section 2, for identical parallel beam sources the effective dose equivalent for PA geometry is slightly smaller than for AP geometry. But results here indicate that dosimeters on the chest or the back will respond the same to sources they "see." Therefore, if dosimeters placed on the front and back are calibrated the same, the dosimeter on the back will slightly overestimate effective dose equivalent for PA exposures.

3.3.3 LAT Exposures

Figure 13 shows contour plots of normalized dosimeter response for radiation striking the phantom from the right side (LAT geometry). Dosimeters facing this radiation (dosimeters located within the region labeled "Back" to "Right" to "Front" in these plots) show very similar responses ranging from approximately

0.9 to 1.1 for all energies considered. This result is essentially the same as the AP and PA exposures.

The LAT exposure geometry is interesting because many of the dosimeters on the front and back of the phantom are exposed to radiation incident from large angles, that is from radiation entering the dosimeter from the side. Traditionally, an ideal dosimeter has been considered as one having an isotropic angular response. And, if dosimeters have an isotropic response and are not shielded by the body, their responses would theoretically be the same to photon beams regardless of the exposure angle (when considering only primary incident radiation). In this study the simulated dosimeters (air-filled spheres) were isotropic. Thus, the reading for a dosimeter on the chest exposed to AP beams would be expected to be the same as the reading for the same dosimeter exposed to LAT beams, as long as photon scattering was negligible.

The ratios of dosimeter readings (actual, not normalized values) for dosimeters located mid-torso at Z = 41 cm under LAT geometry to that under AP geometry are 0.8, 0.95, and 1.06 for the 0.08, 0.3, and 1.0 MeV photon beams, respectively. This difference is due to variations in photon scattering effects for the differing photon energies. Photons entering the dosimeter volume from the side (LAT) pass through the volume and out the other side. Photons entering the dosimeter volume from the front (AP) pass through the volume and then strike the phantom, where scattering can occur. Compton scattering causes lower energy AP photons to be scattered in both the forward and backward directions, the backscattered photons add to the dosimeter reading. Higher energy AP photons are more likely to be scattered in the forward direction, away from the dosimeter volume. Of course LAT beams that strike the phantom from the side are also scattered forward and backward. However, only the forward scattered photons pass through the dosimeter on the chest. Thus, the ratio LAT/AP is greater than unity for 1.0 MeV photons and is smaller than unity for 0.08 MeV photons.

Earlier results (Section 2) indicated that effective dose equivalent for the LAT geometry was about 1/2 to 2/3 of that for the AP geometry, depending on photon energy. When radiation is incident from the sides, effective dose equivalent—because it is the weighted sum of dose equivalents to organs and tissues situated mostly deep inside the body—is significantly influenced by attenuation in

intervening body tissues. Thus, an isotropic dosimeter calibrated for AP exposures would overestimate effective dose equivalent for LAT exposures by a factor of about two at low energies and a factor of about 1.5 at high energies.

3.3.4 Overhead Exposures

Contour plots of normalized dosimeter response for radiation striking the phantom from overhead are shown in Figure 14. The influence of the female breasts are clear because they shield some of the dosimeters located on the front of the torso below the breasts. Backscatter from the skull causes dosimeters on the head to have slightly higher responses than those on the torso. The maximum difference is about 20%, 15%, and 8% for 0.08, 0.3, and 1.0 MeV photon beams, respectively. Dosimeters on the legs are partially or completely shielded by the body depending on distance from the top of the leg. Dosimeters on the front of the legs at about thigh level show relative dosimeter response ranging from about 0.1 (at 0.08 MeV) to about 0.5 (at 1.0 MeV). The effective dose equivalent from the overhead geometry is substantially less than AP geometry, ranging from about 15% of the AP value at 0.08 MeV to about to 30% at 1.0 MeV. The lower effective dose equivalent is due to the significant photon backscatter by the skull. However, an isotropic dosimeter located on the chest responds about the same to both overhead and AP beams. Thus, such a dosimeter would overestimate effective dose equivalent from overhead sources by a factor of about three to seven depending on photon energy.

An example of overhead exposures at nuclear power plants is work performed while standing under the tube sheet during steam generator inspection. Under these circumstances the NRC considers a dosimeter worn on the chest or waist to be unacceptable, and requires a dosimeter on the head. As noted above, the chest-worn dosimeter—when used as a measure of effective dose equivalent—over-responds. Thus, the approach required by NRC will most probably significantly overestimate a worker's effective dose equivalent. (Of course, special dosimeters may still be needed to monitor eye dose during such exposures.)

3.3.5 Underfoot Exposures

Contour plots of normalized dosimeter response for radiation striking the phantom from underfoot are shown in Figure 15. Dosimeters located on the head are largely shielded by the torso, and thus show quite small readings. In contrast, dosimeters on the legs and most of the torso show fairly uniform response, ranging from about 0.7 to 1.2, for the entire range of photon energies studied. Dosimeters placed on the legs receive a significant contribution from backscatter from the leg bones. Considering the effective dose equivalent for underfoot exposures is about 1/3 of that for AP exposure (25-40% depending upon energy), a chest-worn dosimeter also overestimates effective dose equivalent.

3.3.6 Arbitrary Exposures

To illustrate the effects of a photon beam neither normal to or parallel to the body's main axis, a beam incident on the front of the phantom from the upper right was selected (45° polar and 45° azimuthal). Contour plots of normalized dosimeter response for radiation striking the phantom from this direction are shown in Figure 16. Similar to the exposure geometries discussed above, dosimeters over a large area of the body facing the radiation show responses within about 10% of each other. Elsewhere on the phantom there are very steep response gradients. Dosimeters on well shielded areas of the phantom—such as the left rear of the torso—read only a small fraction of the chest dosimeter (< 10% at low energy, about 20% at high energy).

Dosimeters shielded by the body from these "double-slant" incident beams show more complicated variations in response than those shielded from perpendicularly incident geometries. However, inspection of these contour plots relative to the incident photon direction indicates that variations in response can be explained by attenuation and backscatter considerations.

3.4 Conclusions on Dosimeter Positioning

The dosimeter response calculations for AP, PA, LAT, overhead, underfoot, and arbitrary exposure geometries provide sufficient data to arrive at some general conclusions on dosimeter placement:

- Dosimeter location has little influence on response, provided the dosimeter directly "sees" the radiation source. For radiation incident from the front half-plane (AP), a dosimeter placed on the mid-torso will be representative of all other front-of-body locations. Similarly, a dosimeter placed on the back will accurately represent the response of other back-of-body dosimeters to rear-incident (PA) beams.

- Due to body shielding, dosimeters "shadowed" by the body may under-respond by up to 90% at low energies (0.08 MeV) and 50% at high energies (1.0 MeV). For sources overhead or underfoot, the under-response can be even greater.

- In order to minimize radiation dose, considerable advance planning goes into all work at nuclear power plants that involve large personnel exposures. This means that workers entering a radiation area are aware of general dose rates in the work zone, and the magnitude and location of high dose rate locations ("hot spots"). Thus, radiation protection personnel are generally in a position to know in advance if a dosimeter worn on the front of the body will be "shadowed" from significant radiation sources. Usually the principal sources of a worker's radiation exposure are nearby sources he or she is facing as they work. Thus, under most circumstances a single dosimeter worn on the front of the body is a good measure of radiation exposure.

- Occasionally radiation sources in a work location are not well defined, or in the course of performing a job, workers may move unsystematically relative to several significant radiation sources. Under these situations, preventing a "shadowed" dosimeter calls for using two dosimeters, one on the front and one on the back. Two dosimeters are adequate because for all beam sources (even directly overhead and underfoot) a dosimeter at the center of the torso (chest or back) that "sees" the radiation is a very good

indicator of effective dose equivalent. Clearly, such an approach has to be coupled with a proper algorithm to interpret dual responses and convert them to effective dose equivalent.

- Additional dosimeters beyond either the single front-worn dosimeter or a two dosimeter combination (front and back) is not recommended for whole body exposures, regardless of exposure angle. The requirement to place dosimeters at the point of highest dose is generally unnecessary. It can, depending on location, substantially overestimate the effective dose equivalent. Multi-badging beyond a dosimeter on the front and one on the back of the body should be abandoned except for rare cases (e.g., eye exposure).

The above conclusions apply to whole body exposures to broad parallel photon beams, the source geometry most commonly encountered in the workplace. Dosimeter response to isotropic point sources located close to the body were also investigated. Generally, dosimeter response varies according to the inverse-square of the source-to-dosimeter distance, and is more sensitive to the distance than effective dose equivalent.

For point sources, a dosimeter placed at the center of the torso may overestimate or underestimate effective dose equivalent depending on both source-to-dosimeter and source-to-organ distances. It is obvious that the worst case is for a point source in contact with the body. There are also cases[13,14] in which other factors—such as eye or skin dose—become more limiting than whole body effective dose equivalent. Additional information on our findings from point source exposures are presented in the next section.

4.0 RELATING SURFACE FLUENCE MEASUREMENTS TO EFFECTIVE DOSE EQUIVALENT

4.1 Effective Dose Equivalent Algorithms—An Overview

This section examines several algorithms for calculating external effective dose equivalent based on dosimeter response. An effective dose equivalent algorithm should meet several criteria if it is to be readily adopted by the nuclear power industry.

1. It should be based on a comprehensive, scientific assessment of effective dose equivalent under circumstances that bound the conditions expected to be encountered in the workplace. That is, it should apply over a broad range of photon energies and for beam and point sources whose radiation strikes the body from any and all directions.

2. It should be simple and universally applicable. That is, it should not require adjustments or correction factors that depend upon energy, beam direction, source size, etc. Despite differences in radio-sensitivity of some organs, it should apply to both males and females. It should be logical, easy to explain, and easy to derive.

3. It should be demonstrably conservative. That is, there should be no common exposure circumstances (photon energy, source type, incidence angle, etc.) where the algorithm seriously under-predicts effective dose equivalent. (Acceptable uncertainties in effective dose equivalent determinations are discussed below.)

In the sections below we examine several algorithms for determining effective dose equivalent. Based on the results presented in Section 3, these algorithms use the results of dosimeters placed on the front (chest) and rear (back) of the torso. Exposure geometries evaluated include parallel beam sources (AP, PA, LAT, overhead, underfoot, and arbitrary) and various point sources located on (or very close to) the body.

Three simple effective dose equivalent algorithms* were evaluated based on their ability to convert front dosimeter readings (R_{Front}) and back dosimeter readings (R_{Back}), for a variety of exposure geometries, to accurate effective dose equivalents.

1. Algorithm 1 (A1) uses the reading from a single dosimeter worn on the chest. This is the algorithm currently used in the industry.

   A1: $H'_E = R_{Front}$

2. Algorithm 2 (A2) uses the average of two dosimeter readings, one worn on the chest and one on the back.

   A2: $H'_E = Avg\ (R_{Front} + R_{Back}) = (R_{Front} + R_{Back}) / 2$

3. Algorithm 3 (A3) uses two dosimeter readings but weights the highest reading.

   A3: $H'_E = [Max\ (R_{Front}\ or\ R_{Back}) + Avg\ (R_{Front} + R_{Back})] / 2$

   where Max stands for the greatest of the two dosimeter readings.

Table 8 summarizes effective dose equivalent and front and back dosimeter response for a variety of source types, geometries, and photon energies. The effective dose equivalents are gender-averaged results obtained using the MCNP code on the male and female (Cristy) phantoms. The dosimeter responses are from using the MCNP code on the hermaphroditic phantom. Table 9 shows ratios of the estimated effective dose equivalent as calculated by the algorithms (H'_E) to the actual effective dose equivalent (H_E) from Table 8. A comparable table in which the data are not gender-averaged is presented in Appendix A. Thus, interested readers may examine the differences in how well these algorithms predict effective dose equivalent for males versus females.

The algorithms were evaluated for the extent to which they either underestimate or overestimate effective dose equivalent, as well as for their consistency in this regard. An ideal algorithm should not significantly underestimate effective dose

---

* We did examine other algorithms (root mean square, square root of the sum of the squares, etc.) and found they yielded comparable values. We settled on these three because they are simple and logical. It is important to realize there are significant uncertainties in radiation dosimetry. These uncertainties mean it is not worthwhile to try to "fine tune" an algorithm.

Table 8. Calculated Effective Dose Equivalent and Front and Back Dosimeter Values for a Hermaphroditic Phantom

Parallel beam sources are in units of E-15 rad-cm squared per photon
Point sources are in units of E-15 rad per photon

Source Type	Source Geometry	0.08 MeV Photons			0.3 MeV Photons			1.0 MeV Photons		
		Eff. Dose	Dosimeter Reading		Eff. Dose	Dosimeter Reading		Eff. Dose	Dosimeter Reading	
		Equiv.	Front	Back	Equiv.	Front	Back	Equiv.	Front	Back
Parallel Beams	AP	0.48	0.55	0.06	1.60	2.01	0.51	4.56	5.58	2.30
	PA	0.40	0.07	0.53	1.30	0.51	1.99	4.05	2.29	5.56
	LAT	0.23	0.42	0.43	0.91	1.90	1.92	3.24	5.69	5.87
	Overhead	0.12	0.35	0.34	0.49	1.57	1.53	1.91	5.08	4.96
	Underfoot	0.09	0.34	0.33	0.41	1.51	1.48	1.46	4.90	4.86
	Arbitrary	0.31	0.51	0.03	1.17	2.01	0.31	3.80	5.65	1.89
Point Sources at Z = 41 cm (mid-torso height)	X = 0, Y = -44 cm	1.70	3.52	0.17	5.76	12.90	1.09	17.28	39.57	5.70
	X = 44, Y = -44 cm	0.78	1.25	0.09	2.72	4.76	0.65	8.52	13.55	3.24
	X = 44, Y = 0 cm	0.82	0.81	0.75	3.28	4.36	4.20	11.83	15.38	15.26
	X = 44, Y = 44 cm	0.62	0.10	1.20	2.05	0.70	4.65	6.79	3.33	13.44
	X = 0, Y = 44 cm	1.34	0.13	2.47	4.33	1.17	8.10	13.46	5.38	36.34
Point Sources at Z = 6 cm (hip height)	X = 0, Y = -44 cm	1.46	1.66	0.07	4.91	6.28	0.59	14.72	18.11	3.09
	X = 44, Y = -44 cm	0.68	0.89	0.04	2.41	3.49	0.39	7.59	10.17	2.35
	X = 44, Y = 0 cm	0.51	0.40	0.41	2.25	2.21	2.32	8.64	8.47	9.07
	X = 44, Y = 44 cm	0.49	0.05	0.89	1.69	0.39	3.36	5.68	2.27	9.88
	X = 0, Y = 44 cm	0.97	0.08	1.57	3.24	0.65	6.80	10.27	3.18	17.56

Table 9. Performance of Dosimeter Algorithms for Predicting Effective Dose Equivalent

		Ratio of EDE Calculated by Dosimeter Algorithms to "True" EDE Calculated by Monte Carlo Code								
		0.08 MeV Photons			0.3 MeV Photons			1.0 MeV Photons		
Source Type	Source Geometry	Algorithm 1	Algorithm 2	Algorithm 3	Algorithm 1	Algorithm 2	Algorithm 3	Algorithm 1	Algorithm 2	Algorithm 3
Parallel Beams	AP	1.14	0.63	0.89	1.25	0.79	1.02	1.23	0.87	1.05
	PA	0.17	0.76	1.05	0.39	0.96	1.25	0.56	0.97	1.17
	LAT	1.82	1.83	1.84	2.10	2.11	2.11	1.76	1.79	1.80
	Overhead	2.25	2.24	2.24	2.49	2.47	2.48	2.04	2.03	2.04
	Underfoot	3.61	3.57	3.60	3.66	3.64	3.65	3.35	3.33	3.34
	Arbitrary	1.64	0.86	1.25	1.71	0.99	1.35	1.49	0.99	1.24
Point Sources at Z = 41 cm (mid-torso height)	X = 0, Y = -44 cm	2.07	1.09	1.58	2.24	1.22	1.73	2.29	1.31	1.80
	X = 44, Y = -44 cm	1.60	0.86	1.23	1.75	1.00	1.37	1.59	0.99	1.28
	X = 44, Y = 0 cm	0.99	0.95	0.97	1.33	1.31	1.32	1.30	1.30	1.30
	X = 44, Y = 44 cm	0.16	1.05	1.50	0.34	1.31	1.79	0.49	1.24	1.60
	X = 0, Y = 44 cm	0.10	0.97	1.41	0.27	1.57	2.22	0.40	1.55	2.13
Point Sources at Z = 6 cm (hip height)	X = 0, Y = -44 cm	1.14	0.60	0.87	1.28	0.70	0.99	1.23	0.72	0.98
	X = 44, Y = -44 cm	1.31	0.69	1.00	1.45	0.81	1.12	1.34	0.83	1.08
	X = 44, Y = 0 cm	0.78	0.80	0.80	0.98	1.01	1.02	0.98	1.02	1.03
	X = 44, Y = 44 cm	0.11	0.97	1.39	0.23	1.11	1.55	0.40	1.07	1.41
	X = 0, Y = 44 cm	0.08	0.85	1.24	0.20	1.15	1.63	0.31	1.01	1.36

equivalent, but neither should it be overly conservative and thereby greatly overestimate the worker's risk. A consistent algorithm can be applied with confidence to unknown geometries or energies, and if necessary can be refined using correction factors to make it more accurate.

Before addressing algorithm performance it is appropriate to define what constitutes acceptable accuracy. Dosimetry measurements are complex, and there are many factors that cause variations and uncertainty in exposure measurement, including photon energy, angle of incidence, dosimeter construction, and readout and calibration procedures. Recognizing this, the International Commission on Radiological Protection has recommended[7] a factor of 1.5 or less at the 95% confidence level for exposures near the maximum permissible levels of 50 mSv (5 rem), or a factor of 2 or less at the 95% confidence level when the annual reported dose is less than 10 mSv (1 rem).

Since the vast majority of nuclear power plant exposures are << 10 mSv, being within a factor of two of the effective dose equivalent is acceptable performance. While a factor of two may seem large, it is important to understand that large variations in dosimetry measurements exist even under carefully controlled conditions. For example, a certified dosimetry laboratory* is allowed to have measurements be within 30% of the true dose delivered to standard dosimeters, and this is under carefully controlled exposure conditions where the photon energy is known.

4.2 Algorithm Performance

AP Exposures

All three algorithms adequately predict effective dose equivalent from beams striking the phantom from the front. Generally, algorithms 1 and 3 slightly overestimate H_E over the entire energy range, except algorithm 3 under-predicts H_E by about 10% at very low photon energies. Because algorithm 2 gives equal weight to the dosimeter reading that is shielded by the body, it under-predicts H_E

* Certified under the National Voluntary Laboratory Accredidation Program (NAVLAP)

over the entire energy range. This under-prediction ranges from about 15% at high energies to about 40% at low energies.

PA Exposures

Of course a single dosimeter worn on the chest (algorithm 1) significantly underestimates effective dose equivalent from rear-incident (PA) beams. Algorithm 1 underestimates H_E by over 80% at low energies. As was the case above, algorithm 2 underestimates H_E over the entire energy range because it gives equal weight to the shielded dosimeter (in this case the one on the front of the torso). However, for PA exposures the underestimation is less, and in fact algorithm 2 yields quite accurate H_E for all the photon energies. Algorithm 3 over-predicts effective dose equivalent over the entire energy range, though this over-prediction never exceeds 25%.

LAT Exposures

Recall that effective dose equivalent is less from lateral beams than either AP or PA beams, due to the body's greater shielding in this orientation. However, because dosimeters are assumed to respond isotropically, all the algorithms overestimate H_E over the entire energy range. In the case of lateral exposures neither the chest nor back dosimeters are completely shielded by the body. Thus, the various algorithm predictions of H_E fall within a narrow range (2%) at each photon energy. Each algorithm over-predicts H_E by about a factor of two (1.8 to 2.1).

The angular response of commercial dosimeters is not isotropic; generally they respond less at large angles. One way to achieve a more accurate assessment of effective dose equivalent from lateral beams would be to tailor the angular response functions of commercial dosimeters. This topic is discussed briefly in Section 4.5.

Overhead and Underfoot Exposures

The effects discussed above for lateral exposures are amplified for overhead and underfoot exposures. The effective dose equivalent from these exposures is even

less because there is more body tissue shielding the critical organs from incident photons. As shown in Table 9, at each energy each algorithm yields almost the same degree of H_E over-prediction. For overhead sources these over-predictions range from about 2.6 to 3.2. For underfoot sources the range is narrower, from about 3.3 to 3.6. Because isotropic dosimeters significantly overestimate H_E from overhead and underfoot sources, tailoring the angular response of dosimeters for these exposure geometries would be particularly valuable.

Arbitrary Geometry Exposure

An arbitrarily chosen irradiation geometry was modeled by assuming beams incident from both polar and azimuthal angles of 45° (striking the front of the torso from the upper right). Recall that for exposures striking the front of the body, effective dose equivalent decreases rapidly as one departs from AP geometry, yet the angular response of an isotropic dosimeter does not change appreciably. Therefore, algorithm 1 always overestimates H_E for all front-incident photon beams, and the overestimation increases as one departs from AP geometry. In the case of this arbitrary geometry, algorithm 1 overestimates H_E by 1.5 to 1.7. Algorithms 2 and 3 do a better job of predicting H_E for the arbitrary geometry. Though algorithm 2 slightly under-predicts H_E over the entire range of photon energies, it yields estimates quite close to the actual effective dose equivalent. This is because it does not give extra weight to the dosimeter facing the incident photons.

Point Source Exposures

Isotropic point sources are not as easy to characterize as beam sources, in part because dosimeter responses are very sensitive to source-to-dosimeter distance. Nevertheless, point sources at different locations near the body are a useful test of dosimeter algorithms. Any dosimeter algorithm adopted by industry should not seriously under-predict H_E from point sources. Table 9 shows how the three algorithms predict effective dose equivalent for ten point sources at various distances from the body, five at mid-torso height (Z = 41 cm) and five slightly above the legs-to-torso junction (Z = 6 cm). These locations on the torso and hips were selected because they are at approximately the "worst case" locations. (Recall from Section 2 that point sources near the gonads (male and female) and

sternum (female) produce the largest effective dose equivalent.) The specific locations of these point sources relative to the centerline (the longitudinal axis passing through the center of the body) is as follows:

- X = 0 cm, Y = -44 cm — centered in front of the body 44 cm (17 in.) from the centerline
- X = 44 cm, Y = -44 cm — in front of the body and to the left
- X = 44 cm, Y = 0 cm — on the left side of the body 44 cm from the centerline
- X = 44 cm, Y = 44 cm — in back of the body and to the left
- X = 0 cm, Y = 44 cm — centered in back of the body 44 cm from the centerline.

For point sources near or in contact with the body, the inverse-square law can be applied to both source-to-dosimeter and source-to-organ distances to explain the H'_E/H_E ratios listed in Table 9. When point sources are located the same height as the dosimeters (Z = 41 cm), then only algorithms 2 and 3 do a reasonable job of predicting H_E for all five source locations. As the point source moves from the front and side of the body to the rear, the single dosimeter of algorithm 1 becomes shielded by the body and significantly under-predicts effective dose equivalent.

When the point sources are located at hip height (Z = 6 cm) but the dosimeters are located on the torso and the back (Z = 41 cm), the calculations of H_E become even more complex. In this case the point sources are close to the organs that dominate H_E (the gonads), but are a considerable distance from the dosimeters. As in the case above, as the point source moves from the front and side of the body to the rear, the single dosimeter of algorithm 1 significantly under-predicts effective dose equivalent. Algorithm 1 accurately predicts H_E over the entire energy range as long as the point source is on the front or side of the body. However, algorithm 1 under predicts H_E by as much as 90% as the point source moves to the back, away from the front dosimeter. Algorithms 2 and 3, because they factor in the contribution of the rear dosimeter, accurately predict H_E over a very broad range of photon energies and particle locations.

As discussed in Section 2, for females effective dose equivalent is highest when the point source is on the front of the body near the sternum (about Z = 41 cm). For males the highest effective dose equivalent occurs when the point source is on the front of the body near the gonads (about Z = 6 cm). With these differences in mind, one might recommend that female workers wear their dosimeter(s) at chest or mid-back level, while males wear their dosimeter(s) at waist level. In

this way, the uncertainties in calculating effective dose equivalent due to point sources near or in contact with the breasts (female) or gonads (male) might be minimized. Such placements would have very little effect on the effective dose equivalent calculated for beam sources.

It should be recognized, however, it is quite unlikely that point sources typically encountered in a nuclear power plant will produce a significant effective dose equivalent. Reece et al[2] demonstrated that, for a 75 μCi-hour* exposure to a ^{60}Co point source in contact with the torso at the worst locations (on the sternum for the female and on the gonads for the male), effective dose equivalent would be only about 0.1 mSv (10 mR). (The current dose limit is 50 mSv (5,000 mR) per year). Other locations on or near the body will produce an effective dose equivalent significantly lower.

4.3 Effective Dose Equivalent Measurements Made on a Physical Phantom

In this section we present the results of a series of radiation dose measurements made on a human phantom. This phantom is a physical (rather than mathematical) model of a male human torso from the upper thighs to the head, but with no arms. The phantom used was a RANDO phantom.** It is made of a human skeleton encased in tissue-equivalent material. The phantom (Figure 17) is made up of 34 slabs which stack together to form the simulated human torso. Each slab contains small holes on a 3 cm by 3 cm grid that are filled with either a thermoluminscent dosimeter (TLD) chip or a tissue-equivalent plug. The holes have been mapped and grouped into corresponding human organs. (This and other phantoms are described in reference 15.) The phantom was subjected to known radiation fields from ^{60}Co and ^{137}Cs NIST*** traceable sources in a controlled laboratory environment, and to actual workplace radiation fields at a nuclear power plant. Following these exposures, the doses

---

* 75 μCi-hours is the current Nuclear Regulatory Commission guideline for the maximum allowable exposure to a "hot particle."

** RANDO stands for radiation analog dosimetry. The phantom was made by Alderson Research Laboratories, Inc. of Stamford, CT, now out of business. Similar phantoms are presently available from The Phantom Laboratory, Inc. (Salem, NY).

*** National Institute of Standards and Technology, Gaithersburg, MD.

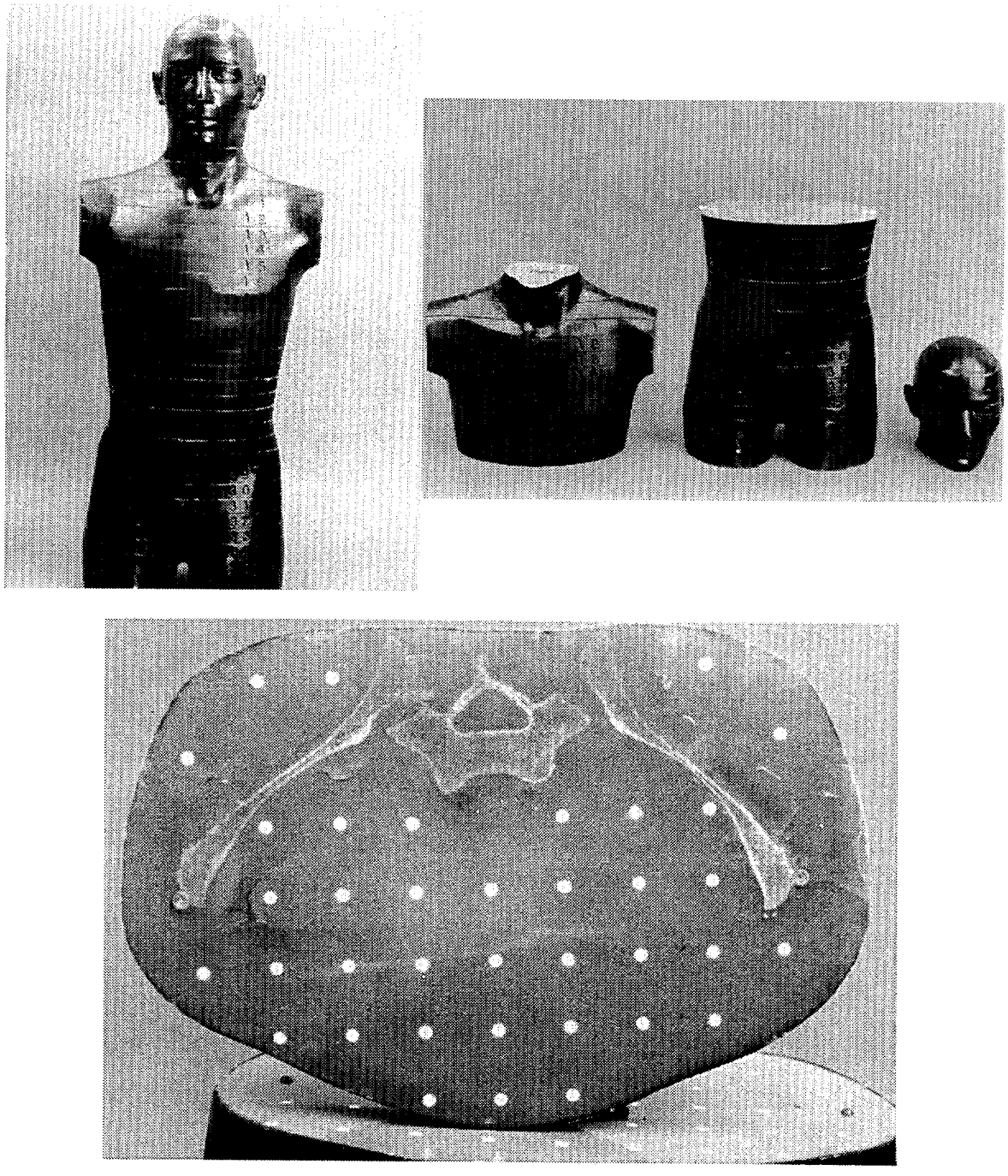

Figure 17. Construction of the RANDO phantom.

measured by TLDs imbedded in the phantom were summed to yield a measured effective dose equivalent. The effective dose equivalent as calculated using the Monte Carlo method (see Section 2) was benchmarked against these laboratory measurements. Separate dosimeters located on the phantom's front and back were processed, and these measured doses were adjusted by the algorithms. The effective dose equivalents estimated from the algorithms were compared to the measured values for both the laboratory and power plant exposures.

4.3.1 Laboratory Measurements

A series of radiation exposure measurements were made on a RANDO phantom at Battelle Pacific Northwest Laboratories (Richland, WA). The first measurements were made early in the study to assure Monte Carlo calculations using the MCNP computer code were generally correct. A ^{60}Co source* calibrated by NIST to produce 2.16 rad per hour at 1 meter (using ANSI 6.1.1-1977[6] fluence-to-dose conversion factors**) was placed 1 meter from the chest of the phantom for 10 hours. The phantom was loaded with more than 200 TLDs. From the TLD readings and individual TLD calibration factors, the dose at each sampling location was calculated, and the organ doses were calculated by weighting the TLD doses by volume fraction of the organ.[16] Table 10 lists the organ doses calculated by MCNP for the Cristy[4] phantoms (in rad per photon emitted), the calculated dose in rad for the total photon fluence, the measured organ dose based on TLD measurements, and the ratio of the measured organ doses in the RANDO phantom to the calculated organ doses in the Cristy phantom. The RANDO and the Cristy phantom were assumed identical—no attempt was made to directly model RANDO.

---

* ^{60}Co emits two photons, 1.17 MeV and 1.33 MeV.

** The 1977 ANSI fluence-to-dose conversion factors have been supplanted by a 1991 version. For ^{60}Co photon energies the differences in the fluence-to-dose conversion factors between the 1977 and 1991 versions are not significant.

Table 10. Measured and Calculated Organ Doses for a ^{60}Co Point Source Exposure 1 Meter from the Chest of a RANDO Phantom

	MCNP Calculation of rad/photon (x 10^{15})	Calculated Dose (rad)	Measured Dose (rad)	Ratio of Measured to Calculated
Adrenals	2.41	10.5	10.3	0.98
Bone Surface	2.23	9.7	10.8	1.11
Brain	2.31	10.1	10.5	1.04
Breast	4.90	21.4	18.7	0.88
Gall Bladder	3.55	15.5	16.8	1.09
Heart	3.68	16.0	15.4	0.96
Kidneys	2.12	9.2	10.3	1.11
Liver	3.41	14.9	15.9	1.07
Lower Large Intestine	3.04	13.3	13.8	1.04
Lung	3.32	14.5	14.1	0.97
Ovaries	2.79	12.2	15.0	1.23
Pancreas	3.05	13.3	15.5	1.17
Red Bone Marrow	2.17	9.5	11.4	1.20
Small Intestine	3.04	13.3	15.4	1.16
Spleen	2.50	10.9	11.7	1.07
Stomach	3.76	16.4	16.4	1.00
Testes	3.66	16.0	18.8	1.18
Thymus	4.25	18.5	16.1	0.87
Thyroid	3.74	16.3	17.1	1.05
Upper Large Intestine	3.33	14.5	15.1	1.04
Uterus	2.87	12.5	11.7	0.94
Average Ratio				1.06
Effective Dose Equivalent		16.9	15.5	0.92
Front Dosimeter Reading			21.6	
Back Dosimeter Reading			7.4	

The agreement between measured and calculated organ dose equivalents is generally excellent. The largest differences, on the order of ±12%, occur in tissues difficult to measure because of their distended nature (such as bone surfaces) or because of their small size (such as the thymus). Considering the experimental errors in TLD measurements and that RANDO and Cristy phantoms differ in many small ways, the agreement between the experiments and calculations is quite good. These differences have a relatively small impact on the assessment of effective dose equivalent, and the excellent agreement validates the use of MCNP to calculate effective dose equivalent.

Measurements were also performed on the RANDO phantom using a ^{137}Cs source* calibrated to deliver 2.15 rad per hour at 1 meter. Table 11 presents the organ doses calculated for the Cristy phantom using MCNP, calculated organ doses for the total fluence delivered for the experiment, organ doses calculated from TLD readings, and the ratio of measured to calculated doses for ^{137}Cs exposure.

Again, the agreement between measured and calculated is excellent. While a slight negative bias is shown in these data, a slight positive bias was shown in the ^{60}Co exposures. The cause of these small systematic biases is not known, but could be from experimental error in either TLD calibration or source calibrations, slight differences in phantom position, or differences between the model and the phantom itself. An assessment of the dosimeter algorithms using these laboratory data are presented in Section 4.4 below.

4.3.2 Field Measurements

Field measurements at a nuclear power plant were also performed to assess how the algorithms would work in a mixed or unknown gamma field. The exposures were much the same as the controlled laboratory experiments, except the sources are not well defined.

The RANDO phantom was used to measure effective dose equivalent from exposure to power plant radiation fields.** The phantom was loaded with TLD packets, each packet containing three TLDs. (Some field measurements used 50 packets, others used 100 packets.) The TLD packets were distributed through the phantom to measure gamma doses at the locations of significant organs. Also,

---

* ^{137}Cs emits a 0.662 MeV photon.

** An attempt was made to fully model the power plant radiation fields by directly measuring their angular variations using a shielded, high-purity germanium, gamma spectrometer. Unfortunately, the unfolding of the incident gamma spectra from the responses of the germanium detector proved much more difficult than anticipated. We were unable to complete the radiation field modeling so the spectrometry data are not reported herein.

four TLD packets, configured to measure shallow dose, were attached to the phantom at waist level, one on the front, one on the back, and one on each side.

Table 11. Measured and Calculated Organ Doses for a ^{137}Cs Point Source Exposure 1 Meter from the Chest of a RANDO Phantom

	MCNP Calculation of rad/photon (x 10^{15})	Calculated Dose (rad)	Measured Dose (rad)	Ratio of Measured to Calculated
Adrenals	1.24	499	473	0.95
Bone Surface	1.28	517	520	1.01
Brain	1.33	538	479	0.89
Breast	2.96	1,194	914	0.77
Gall Bladder	2.11	853	850	1.00
Heart	2.20	886	750	0.85
Kidneys	1.14	458	469	1.02
Liver	2.01	813	747	0.92
Lower Large Intestine	1.44	582	624	1.07
Lung	1.95	786	650	0.83
Ovaries	1.65	664	650	0.98
Pancreas	1.77	714	746	1.05
Red Bone Marrow	1.22	493	500	1.01
Small Intestine	1.98	798	697	0.87
Spleen	1.42	572	nm	
Stomach	2.27	914	801	0.88
Testes	2.23	900	875	0.97
Thymus	2.62	1,056	836	0.79
Thyroid	2.25	909	845	0.93
Upper Large Intestine	1.98	798	793	0.99
Uterus	1.71	691	521	0.75
Average Ratio				0.93
Effective Dose Equivalent		842	734	0.87
Front Dosimeter Reading			1,028	
Back Dosimeter Reading			282	

nm = not measured

The phantom was positioned in each measurement location for many hours, so that the dose delivered was usually greater than 100 mrad, ensuring good statistical agreement among TLDs within a packet.

Effective dose equivalent measurements were performed at three locations at the R. E. Ginna nuclear power station, a pressurized water reactor operated by Rochester Gas and Electric Corporation. Areas of significant gamma radiation were chosen.

1. Location 1 was in the reactor containment building, approximately 10 feet (3 m) in front of the personnel hatch. Hand-held survey meter readings indicated a field of 20 mR/h at that location. A neutron survey meter read 50 mrem/h, but the neutron field will have negligible effect on the TLD readings. The phantom was positioned facing the center of the containment building. Effective dose equivalent for this exposure, as measured by the phantom's internal dosimeters, was 75.4 mrad.

2. Location 2 was in the charging pump room, also in the auxiliary building. The phantom was positioned halfway between charging pump A and charging pump B, with the phantom's right side facing the former and its left side facing the latter. Survey readings on the surface of the phantom were as follows:

front	13	mR/h
right side	8.7	"
back	7.0	"
left side	9.7	"

   Effective dose equivalent for this exposure, as measured by the phantom's internal dosimeters, was 147.7 mrad.

3. Location 3 was near chemical volume control tank C in the auxiliary building basement. The front of the phantom was positioned 28 inches (71 cm) from the tank, in a corner of the room, with the nearest wall about 50 inches (127 cm) from the right shoulder. Survey readings on the surface of the phantom were as follows:

front	24	mR/h
right side	20	"
back	3	"
left side	16	"

   Effective dose equivalent for this exposure, as measured by the phantom's internal dosimeters, was 257.9 mrad.

4.4 Algorithm Assessments and Recommendations

In this section the dosimeter data from the RANDO phantom measurements are used to test the effective dose equivalent algorithms presented in Section 4.1. The results are summarized in Table 12.

Table 12. Algorithm Performance in Estimating Effective Dose Equivalent Measured in the RANDO Phantom

Exposure Type	H_E Measured (mrad)	Front Dosimeter (mrad)	Back Dosimeter (mrad)	H'_E / H_E * for Algorithm 1	2	3
Laboratory						
^{60}Co	15.5	21.6	7.4	1.4	0.9	1.2
^{137}Cs	734	1,028	282	1.4	0.9	1.1
Field						
Location 1	75.4	141.8	39.4	1.9	1.2	1.5
Location 2	147.7	194.6	85.3	1.3	0.9	1.1
Location 3	257.9	416.7	155.2	1.6	1.1	1.4

* H'_E = effective dose equivalent as calculated by the algorithm
H_E = measured effective dose equivalent

The ratios of calculated to measured effective dose equivalent ranged from a low of 0.9 to a high of 1.9. All algorithms were acceptable, that is they predicted the measured effective dose equivalent within ICRP guidelines.[7] Algorithm 1 (based on a single front-worn dosimeter) and algorithm 3 (based on weighting the front-worn dosimeter) always over-predicted the effective dose equivalent. Overall, algorithm 2 (a simple average of the front and back dosimeters) provided the best predictions of the measured values. For this limited assessment it never underestimated H_E by more than 10% or overestimated by more than 20%.

Based on these results, utilities not wishing to change their current dosimetry practices to improve the accuracy of their H_E assessments, can continue the practice of using a single dosimeter for routine applications. They can be confident that the single dosimeter approach when used under routine nuclear

power plant exposure conditions has not underestimated effective dose equivalent in the past, and will not do so in the future. Utilities may wish to recommend that women wear their single dosimeters on the chest and men wear theirs on the waist. Such a practice may be beneficial in the unlikely event of exposure to the breasts or gonads from a highly radioactive particle. Though the practice will have no bearing on the effective dose equivalent calculated for routine parallel beam sources.

Utilities may want to examine the cost/benefit of using an algorithm based on readings from both a front and back dosimeter. Based on the results of Table 12, single dosimeter assessments of effective dose equivalent could easily be 30% (or more) greater than the true effective dose equivalent. Utilities should examine their annual collective exposures to see how the cost of analyzing twice as many dosimeters compares to the benefits in reporting a lower, and more accurate, collective dose. In recent years in the United States, personnel exposures to power plant workers have been averaging about 3 mSv (300 mR) per person per year. Using a two-dosimeter algorithm could reduce this value to about 2 mSv (200 mR), lowering reported exposures by about 100 mSv (10 rem) per year per 100 radiation workers. Many utilities spend $5,000 or more to save one person-rem, suggesting a two dosimeter approach may be beneficial.

It can be argued that a revised calibration factor be used on a single, front-worn dosimeter that would reduce the reported dose by (say) 30%. However, special circumstances (such as PA beams) where the body effectively shields the front-worn dosimeter would have to be evaluated and addressed by utilities selecting this approach. Evaluating such circumstances may require detailed radiation surveys and careful analysis of work practices. Use of both a front and back dosimeter on a worker would eliminate special circumstance concerns, saving the cost of such evaluations.

It has been reported that workers may be required to wear as many as 12 dosimeters for a single work task under unusual exposure conditions.[13] This report has shown that this practice—as well as the practice of trying to place dosimeters on the body at the perceived point of highest dose—are not necessary. At most only two dosimeters are needed to satisfactorily assess effective dose equivalent. No special placements are required, except that one dosimeter

should be placed on the front of the body and another on the back. Of course, unusual circumstances—exposure to the eyes, working behind a shadow shield, a worker whose head is in a manway opening, etc.—may justify special dosimetry.

4.5 Comments on the Angular Response of Dosimeters

Section 2 describes how effective dose equivalent varies with photon angle of incidence. These variations are summarized in Figures 4 and 5. Section 4 discusses how effective dose equivalent algorithms derived from the response of isotropic dosimeters significantly overestimate H_E as the incidence angle departs from normal to the body's major axis (AP and PA). For gender-averaged exposures, this over-prediction is about a factor of two for radiation striking the body from the side (LAT) and almost a factor of four from underfoot sources.

Actual dosimeters are not isotropic, but instead show directional dependence. That is, they read less when exposed to a source whose radiation strikes them from a large angle than they do when exposed to the same source exposed "head on" (AP). Both the 1983 and 1993 ANSI dosimetry testing standards[17,18] require some angular response measurements, but the standards and regulatory guides have generally been silent about how to deal with angular response variations. The angular response issue has been examined and an empirical equation has been derived which relates effective dose equivalent, photon energy, and radiation angle.[19] The equation is an average of an isotropic response function and a simple cosine function whose curvature depends upon incident photon energy. The equation is valid for energies from 0.01 MeV to 10 MeV. Reference 19 presents a detailed discussion of the angular response issues. The results presented therein can be used to:

- improve estimates of effective dose equivalent
- serve as a basis for redesigning dosimeter performance testing and calibration methods
- design dosimeters to more appropriately respond to directional variations.

5.0 CONCLUSIONS AND RECOMMENDATIONS

5.1 Summary of Volumes 1 and 2

We have demonstrated, using industry standard computer codes and anthropomorphic phantoms, that one can accurately assess effective dose equivalent from exposures to both beam and point sources. By modeling isotropic dosimeters on the surface of the phantoms, these tools were also used to understand how dosimeter placement will influence effective dose equivalent assessments. The data summarized in this report and the earlier companion volume[2] can be used by advisory groups to establish recommendations for monitoring workers exposed to external radiation fields. Applying these data to the practical problems of dosimetry placement and dose assessment can improve present effective dose equivalent measurement practices, and yield more accurate assessments of the potential risks from ionizing radiation exposure.

Important conclusions from these two EPRI reports are as follows.

- For equivalent energy flux, lower energy photons always produce lower effective dose equivalents. This is in contrast to the 1977 flux-to-dose conversion factors widely used in the industry (reference 6) which predict that dose decreases with decreasing energy to about 80 keV, and then increases again. In fact, effective dose equivalent decreases monotonically with energy.

- For equal beam intensities, radiation striking the body from the front produces the greatest effective dose equivalent. Beams striking the rear of the torso produce the next highest effective dose equivalent, with H_E falling significantly as one departs from these orientations.

- For point sources the highest effective dose equivalent for females occurs when the source is in contact with the body on the sternum, and for males when the source is on the gonads. If a ^{60}Co particle was on the body at these locations for the maximum permitted exposure per NRC "hot particle" guidelines, the effective dose equivalent would only be about 0.1 mSv (10 mR), a very small fraction of the exposure limit. Thus, point

sources—whose flux falls as the reciprocal of the distance squared—are relatively innocuous compared to the uniform exposure from beams.

- It may be a good practice for women to wear their dosimeter on the chest and men to wear theirs on the waist. This would yield a more accurate measure of effective dose equivalent in the event of exposure to the breasts or gonads from a highly radioactive particle. Such a practice would have no effect on the H_E calculated for exposure to routine beam sources in nuclear power plants.

- For broad, parallel radiation beams striking the body from the front (or the back), a dosimeter placed anywhere on the front (or back) of the body from the upper chest to the upper legs (or upper back to upper legs) will yield an accurate measure of effective dose equivalent.

- For atypical exposure situations, such as broad beams from overhead or underfoot, the widespread practice of placing dosimeters on the body proximate to the beam should be abandoned. In these cases the dosimeter response can significantly overestimate the effective dose equivalent. Similarly, the practice of multi-badging workers and selecting the highest dosimeter reading as the exposure of record should be abandoned. Two dosimeters—one on the front and one on the back—are adequate to accurately measure effective dose equivalent. (Of course situations can arise—such as eye exposures—where other than whole body effective dose equivalent must be considered. In these cases special dosimetry may be appropriate.)

- While this work was in progress ANSI adopted a new fluence-to-dose conversion standard which (as discussed in Volume 1) correlate exactly with the results of this study. Using that standard one can calculate effective dose equivalent given detailed knowledge of beam geometry and photon energy. This work extends this concept by providing simple algorithms for assessing effective dose equivalent based on either one or two dosimeter readings. These algorithms do not require knowledge of either source geometry or photon energy. Once there is industry-wide

adoption of the new ANSI standard, more accurate effective dose equivalent assessments will result.

- Any of the simple dosimeter algorithms examined here:
  - front dosimeter only,
  - average of front and back dosimeters, or
  - weighted average of front and back dosimeters,

  will yield acceptably accurate assessments of effective dose equivalent under common radiation exposure situations. However, of these three techniques, the current practice of using a single front-worn dosimeter routinely overestimates effective dose equivalent, though this overestimation falls within acceptable ICRP guidelines.

- Finally, occupational radiation exposure regulations may become more restrictive. If so, utilities may seek ways to more accurately assess effective dose equivalent over the current single-dosimeter technique. In which case it may be desirable in certain work situations to provide workers with two dosimeters, one worn on the front of the torso and one worn on the back. In those situations, a simple algorithm (such as the ones discussed herein) applied to those dosimeter readings will yield an effective dose equivalent that is both numerically lower and more accurate than that yielded by a single dosimeter.

6.0 REFERENCES

1. Title 10 Part 20 of the Code of Federal Regulations, "Standards for Protection Against Radiation," as revised August 21, 1991.

2. W.D. Reece, J.W. Poston, and X.G. Xu, "Assessment of the Effective Dose Equivalent for External Photon Radiation—Volume 1: Calculational Results for Beam and Point Geometries," Electric Power Research Institute, EPRI TR-101909, February 1993.

3. International Commission on Radiological Protection, "Recommendations of the International Commission on Radiological Protection," ICRP Publication 26, Annals of the ICRP, Vol. 1 No. 3, Pergamon Press, 1977.

4. M. Cristy and K.F. Eckerman, "Specific Absorbed Fractions of Energy at Various Ages from Internal Photon Sources," ORNL/TM-8381/V1, April, 1987.

5. Radiation Shielding Information Center, "MCNP 4: Monte Carlo Neutron and Photon Transport Code System," Oak Ridge National Laboratory Report No. CCC-200A, 1991.

6. American Nuclear Society, "American National Standard Neutron and Gamma-Ray Flux-to-Dose-Rate Factors," ANSI/ANS-6.1.1-1977, 1977.

7. International Commission on Radiological Protection, "General Principles of Monitoring for Radiation Protection of Workers," ICRP Publication 35, Pergamon Press, Oxford, 1982.

8. N.E. Hertel, J.C. McDonald, "Methods for the Calibration of Photon Personnel Dosimeters in Terms of the Ambient Dose Equivalent, Radiation Protection Dosimetry, 32(3), pp. 149-156, 1990.

9. C. Austerlitz, B. Kahn, G.G. Eichholz, M. Zankl, and G. Drexler, "Calculation of the Effective Male Dose Equivalent Relative to the Personal

Dose at Nine Locations with a Free Arm Model," Radiation Protection Dosimetry, 36(1), pp. 13-21, 1991.

10. X.G. Xu, "The Assessment of Effective Dose Equivalent Using Personnel Dosimeters," Dissertation for Ph.D. in Nuclear Engineering/Health Physics, Texas A&M University, May 1994.

11. J.H. Hubbell, "Photon Mass Attenuation and Mass Energy-Absorption Coefficients from 1 keV to 20 MeV," Int. J. Appl. Radiat. Isot., 33, pp. 1269-1290, 1982.

12. F.H. Attix, Introduction to Radiological Physics and Radiation Dosimetry, John Wiley & Sons, Inc., New York, 1986.

13. W.D. Reece, L.W. Backenbush, and P.L. Roberson, "Extremity Monitoring: Considerations in Use, Dosimeter Placement, and Evaluation," NUREG/CR-9279, Nuclear Regulatory Commission; 1985.

14. "Limit for Exposure to "Hot Particles" on the Skin," National Council on Radiation Protection and Measurements, Bethesda, MD, NCRP Report No. 106, 1989.

15. "Phantoms and Computational Models in Therapy, Diagnosis and Protection," ICRU Report 48, International Commission on Radiation Units and Measurements, Bethesda, MD, 1992.

16. V.Y. Golikov and V.V Nikitin, "Estimation of the Mean Organ Doses and the Effective Dose Equivalent from RANDO Phantom Measurements," Health Physics, Vol. 56. No. 1, pp. 111-115, 1989.

17. Standard for Dosimetry-Personnel Dosimetry Performance-Criteria for Testing, ANSI Report No. N13.11, American National Standards Institute (New York, NY), 1983.

18. Standard for Dosimetry-Personnel Dosimetry Performance-Criteria for Testing, ANSI Report No. N13.11, American National Standards Institute (New York, NY), 1993.

19. X.G. Xu, W.D. Reece, and J.W. Poston, Sr., "A Study of the Angular Dependence Problem in Effective Dose Equivalent Assessment," Health Physics, Vol. 68, No. 2, February 1995.

APPENDIX A

Table of Algorithm Performance for Males and Females

Section 4 assessed the ability of the dosimeter algorithms to predict effective dose equivalent. The effective dose equivalents used were for either a male physical phantom (RANDO) or a hermaphroditic ("average gender") mathematical phantom. The table that follows shows how well each of the algorithms predict the effective dose equivalent for females and males. These effective dose equivalents were calculated using the detailed mathematical phantoms (developed by Cristy) described in Section 2. These data are presented for completeness; they do not alter the conclusions and recommendations presented in Section 5.

Table A1. Performance of Dosimeter Algorithms for Predicting Effective Dose Equivalents for Females and Males

		Ratio of EDE Calculated by Dosimeter Algorithms to "True" EDE Calculated by Monte Carlo Code																	
		0.08 MeV Photons						0.3 MeV Photons						1.0 MeV Photons					
		Algorithm 1		Algorithm 2		Algorithm 3		Algorithm 1		Algorithm 2		Algorithm 3		Algorithm 1		Algorithm 2		Algorithm 3	
Source Type	Source Geometry	Female	Male	Female	Male	Female	Male	Female	Male	Female	Male	Female	Male	Female	Male	Female	Male	Female	Male
Parallel Beams	AP	1.01	1.31	0.56	0.73	0.79	1.02	1.07	1.51	0.67	0.95	0.87	1.23	1.06	1.46	0.75	1.03	0.90	1.24
	PA	0.15	0.20	0.67	0.86	0.93	1.19	0.34	0.47	0.83	1.15	1.08	1.49	0.48	0.68	0.83	1.16	1.00	1.40
	LAT	1.53	2.24	1.54	2.26	1.54	2.27	1.75	2.61	1.76	2.62	1.76	2.62	1.47	2.19	1.49	2.22	1.50	2.24
	Overhead	2.01	5.31	2.05	5.25	2.06	5.28	2.16	6.16	2.13	6.07	2.15	6.12	1.86	4.66	1.84	4.60	1.85	4.63
	Underfoot	4.05	3.26	4.00	3.22	4.02	3.24	3.84	3.51	3.80	3.47	3.82	3.49	3.31	3.40	3.29	3.38	3.30	3.39
	Arbitrary	1.45	1.88	0.76	0.99	1.11	1.43	1.50	2.00	0.87	1.16	1.18	1.58	1.31	1.72	0.87	1.15	1.09	1.44
Point Sources at Z = 41 cm (mid-torso height)	X = 0, Y = -44 cm	1.68	2.68	0.88	1.41	1.28	2.05	1.66	2.79	0.91	1.52	1.28	2.15	*	*	*	*	*	*
	X = 44, Y = -44 cm	1.32	2.03	0.71	1.09	1.01	1.56	1.42	2.30	0.81	1.31	1.11	1.80	1.29	2.09	0.80	1.29	1.04	1.69
	X = 44, Y = 0 cm	0.78	1.32	0.75	1.27	0.77	1.30	1.04	1.83	1.02	1.79	1.03	1.81	1.03	1.75	1.03	1.74	1.03	1.74
	X = 44, Y = 44 cm	0.14	0.18	0.94	1.17	1.34	1.66	0.03	0.04	1.01	1.33	1.50	1.98	0.42	0.58	1.06	1.47	1.39	1.92
	X = 0, Y = 44 cm	0.09	0.11	0.88	1.09	1.27	1.58	0.23	0.32	0.92	1.27	1.27	1.75	0.34	0.49	1.32	1.89	1.80	2.59
Point Sources at Z = 6 cm (hip height)	X = 0, Y = -44 cm	1.17	1.10	0.61	0.58	0.89	0.84	1.27	1.29	0.70	0.70	0.98	0.99	1.21	1.26	0.71	0.73	0.96	0.99
	X = 44, Y = -44 cm	1.24	1.38	0.65	0.72	0.95	1.05	1.36	1.56	0.75	0.86	1.06	1.21	1.23	1.47	0.76	0.91	0.99	1.19
	X = 44, Y = 0 cm	0.66	0.96	0.67	0.98	0.67	0.98	0.83	1.20	0.85	1.23	0.86	1.25	0.86	1.13	0.90	1.17	0.91	1.19
	X = 44, Y = 44 cm	0.09	0.12	0.86	1.10	1.24	1.59	0.20	0.27	0.97	1.29	1.35	1.80	0.35	0.46	0.94	1.23	1.24	1.62
	X = 0, Y = 44 cm	0.07	0.09	0.76	0.98	1.10	1.42	0.17	0.24	1.00	1.35	1.41	1.91	0.27	0.36	0.89	1.17	1.19	1.58

* = did not calculate

ABOUT EPRI

The mission of the Electric Power Research Institute is to discover, develop, and deliver high value technological advances through networking and partnership with the electricity industry.

Funded through annual membership dues from some 700 member utilities, EPRI's work covers a wide range of technologies related to the generation, delivery, and use of electricity, with special attention paid to cost-effectiveness and environmental concerns.

At EPRI's headquarters in Palo Alto, California, more than 350 scientists and engineers manage some 1600 ongoing projects throughout the world. Benefits accrue in the form of products, services, and information for direct application by the electric utility industry and its customers.

EPRI—*Leadership in Electrification through Global Collaboration*

EPRI TR-101909-V2

Assessment of the Effective Dose Equivalent for External Photon Radiation

Jun 1995

Printed on recycled paper (50% recycled fiber, including 10% postconsumer waste) in the United States of America.